Modern air, englacial and permafrost temperatures at high altitude on Mt. Ortles (3905 m a.s.l.), in the Eastern European Alps

Luca Carturan[1], Fabrizio De Blasi[1,2], Roberto Dinale[3], Gianfranco Dragà[4], Paolo Gabrielli[5], Volkmar Mair[6], Roberto Seppi[7], David Tonidandel[6], Thomas Zanoner[7,8], Tiziana Lazzarina Zendrini[1], Giancarlo Dalla Fontana[1]

[1]Department of Land, Environment, Agriculture and Forestry, University of Padova, Viale dell'Università 16, 35020 Legnaro, Padova, Italy

[2]Consiglio Nazionale delle Ricerche - Istituto di Scienze Polari, c/o Ca' Foscari University of Venezia, Via Torino 155, 30172 Mestre, Venezia, Italy

[3]Ufficio Idrografico, Provincia Autonoma di Bolzano, 39100 Bolzano, Italy

[4]Geo Monitoring Service s.r.l., Vicolo Santa Elisabetta 39, 39040 Varna, Bolzano, Italy

[5]Italian Glaciological Committee, c/o University of Turin, Via Valperga Caluso 35, 10125 Torino, Italy

[6]Ufficio Geologia e Prove materiali, Provincia Autonoma di Bolzano, 39053 Kardano, Bolzano, Italy

[7]Department of Earth and Environmental Sciences, University of Pavia, Via Ferrata 9, 27100 Pavia, Italy

[8]Department of Geosciences, University of Padova, Via Gradenigo 6, 35131 Padova, Italy

Correspondence to: luca.carturan@unipd.it

28   **Abstract**

29   The climatic response of mountain permafrost and glaciers located in high-elevation mountain areas has major

30   implications for the stability of mountain slopes and related geomorphological hazards, water storage and

31   supply, and preservation of paleoclimatic archives. Despite a good knowledge of physical processes that

32   govern the climatic response of mountain permafrost and glaciers, there is a lack of observational datasets from

33   summit areas. This represents a crucial gap in knowledge and a serious limit for model-based projections of

34   future behaviour of permafrost and glaciers.

35   A new observational dataset is available for the summit area of Mt. Ortles, which is the highest summit of

36   South Tyrol, Italy. This paper presents a series of air, englacial, soil surface and rock wall temperatures

37   collected between 2010 and 2016. Details are provided regarding instrument types and characteristics, field

38   methods, data quality control and assessment. The obtained data series are available through an open data

39   repository.

40   In the observed period, the mean annual air temperature at 3830 m a.s.l. was between -7.8 and -8.6°C. The

41   most shallow layers of snow and firn (down to a depth of about 10 m) froze during winter. However melt water

42   percolation restored isothermal conditions during the ablation season and the entire firn layer was found at the

43   melting pressure point. Glacier ice is cold, however only from about 30 m depth. Englacial temperature

44   decreases with depth reaching a minimum of almost -3°C close to the bedrock, at 75 m depth. A small glacier

45   located at 3470 m a.s.l., close to the summit of Mt. Ortles, was also found in cold conditions down to a depth

46   of 9.5 m. The mean annual ground surface temperature was negative for all but one monitored sites, indicating

47   cold ground conditions and the existence of permafrost in nearly all debris-mantled slopes of the summit.

48   Similarly, the mean annual rock wall temperature was negative at most monitored sites, except the lowest one

49   at 3030 m a.s.l. This suggests that the rock faces of the summit are affected by permafrost at all exposures.

50

51

52

53

54

55

1. Introduction

High-elevation mountain areas are complex systems influenced by physical processes occurring in the atmosphere, cryosphere and lithosphere. These processes closely interact and govern the energy and mass balance and climatic response of mountain permafrost and glaciers located at high elevation. Their response to climatic changes has important consequences for i) the stability of mountain slopes and related geomorphological hazards (Huggel et al., 2015; Knight and Harrison, 2023), ii) the thermal regime, water storage and stability of mountain glaciers (Deline et al., 2015), iii) the hydrological balance and water supply from glacierized catchments (Irvine-Fynn and Hubbard, 2017), and iv) the formation and preservation of paleoclimatic archives, such as glacier geochemical records (Gabrielli et al., 2010).

The ongoing atmospheric warming is leading to a deep transformation of these high-elevation systems, which react sensitively to climatic changes. Indeed, the thermal state of the cryosphere is strongly influenced by variations in air temperature, which regulates its energy and mass balance and dynamic behaviour (Harris et al., 2009; Cicoira et al., 2019; Deline et al., 2015). Projections of future global climate indicate further warming in absence of mitigation policies such as the reduction of greenhouse gas emission (IPCC, 2022). For this reason, the current impacts on high-elevation mountain areas are expected to continue and possibly accelerate.

Direct observations of the thermal state and response of high-elevation mountain areas are of great importance. Even though the physical processes that govern the energy and mass balance and climatic response of mountain permafrost and glaciers are known, model-based projections of their future behaviour are subject to large uncertainty. This is because the observational datasets required for model calibration and validation are particularly scarce for these summit areas, where model inputs and results are often poorly constrained and extrapolated, in absence of direct observations (Charbonneau et al., 1981; Machguth et al., 2008; Carturan et al., 2012, Zolles et al., 2019; Kinnard et al., 2022).

Thermal observations in high-elevation mountain areas are also of great value for i) improving knowledge on the air temperature variability (e.g. the so-called elevation-dependent warming, Pepin et al., 2015 and 2022), or the glacier cooling effect (Braithwaite et al., 2002; Carturan et al., 2015; Troxler et al., 2020; Shaw et al., 2023), ii) better understanding the relationship between climatic proxies and meteorological variables (e.g. ice cores, Bohleber et al., 2013), iii) evaluating/improving models (e.g. permafrost distribution models, Boekli et

al., 2012), iv) biological and biogeochemical studies (e.g. Rathore et al., 2018), and v) setting baseline conditions for future studies and trend analyses.

In this paper we present a novel six-year dataset of air, rock, soil surface and englacial temperatures collected between 2010 and 2016 on the summit of Mt. Ortles (46.508° N, 10.541° E, 3905 m a.s.l.), in the eastern Italian Alps. These observations were carried out in the framework of the Ortles Project (ortles.org; Gabrielli et al., 2016), which is an international research project, coordinated by the Byrd Polar and Climate Research Center, The Ohio State University (USA) and the Hydrographic Office of the Autonomous Province of Bolzano, with the aim of extracting ice cores from the Alto dell'Ortles Glacier (Oberer Ortlerferner) to be used for paleoclimatic and paleoenvironmental investigations.

Here we provide a full description of the experimental site, data-collection methods and equipment, raw data processing and final datasets.

2. Site description

Mount Ortles (46.508° N, 10.541° E) is located in the Ortles-Cevedale Mountain Group, which is the largest glacierized area in the Italian Alps (Carturan et al., 2013) and it is the highest peak (3905 m a.s.l.) of South Tyrol (Fig. 1). From a lithological point of view, the summit of Mt. Ortles is mainly composed by dolomites, alternated with dark-stratified limestones and paraconglomeratic limestone levels and breccias. Local outcrops of phyllites rich in quartz and orthogneiss can be found at the base of the mountain (Montrasio et al., 2012). The northern part of the Ortles-Cevedale mountain range is characterised by a continental climate, with scarce annual precipitation (500 mm in the lower valley), which falls mostly in summer. Towards the south, there is an increasing Mediterranean influence and the annual precipitation maxima are in spring and autumn, with cumulative amounts of 900 mm in the lower valleys. In the glaciated areas in the middle of the mountain range, at 3000-3200 m a.s.l., the mean annual precipitation has been estimated between 1400 and 1500 mm (Carturan, 2010; Carturan et al., 2012). Using mass balance observations in the period from 2009 to 2016 it is possible to estimate 1300-1400 mm of annual precipitation on top of Mt. Ortles. However, the snow accumulation and glacier mass balance are highly affected by wind and estimating the actual precipitation is almost impossible at this site. In comparison, the closest weather station (Solda, 1905 m a.s.l.) averaged an annual precipitation of 1090 mm between 1989 and 2019.

The mean annual isotherm of 0°C is located at about 2500 m a.s.l. At the elevation of the glaciers (above 3000 m) the snow cover shows a typical annual cycle, so the accumulation season lasts between October and May, and the ablation season between June and September. On the glaciers, however, snowfalls are frequent during summer, especially above 3300-3500 m. Liquid precipitation is rare on top of Mt. Ortles, but some rain events have been observed in the last 15 years.

Glaciers, glacierets and snowfields cover the Mt. Ortles flanks. Here we describe the Alto dell'Ortles and Hintergrat glaciers, which are the two ice bodies investigated in the Ortles Project. The summit area is almost entirely covered by the Alto dell'Ortles Glacier (Oberer Ortlerferner), which is the highest glacier of South Tyrol, ranging in altitude between 3018 and 3905 m a.s.l. and covering an area of 1.04 km^2 (year 2008). The observed glacier thickness is about 75 m (Gabrielli et al., 2012) and the vertical ice profile encompasses the last ~7 kyr (Gabrielli et al., 2016). This glacier is polythermal, with temperate firn and cold ice underneath (Gabrielli et al., 2012). From geomorphological evidence (trimlines and moraines) it is possible to estimate a maximum Little Ice Age (14th - 19th centuries) area of 2.09 km^2 for this glacier, and a 50% area loss since then. Between 1984 and 2005 the (geodetic) mass balance of the glacier was closer to equilibrium (-0.18 m w.e. y^{-1}) when compared to the majority of glaciers in the Ortles-Cevedale Group in the same period (mean balance rate of -0.69 m w.e. y^{-1}, Carturan et al., 2013). A small glacier, named Hintergrat, covers part of the eastern rocky ridge of Mt. Ortles. The area of this glacier is 0.09 km^2 and its elevation ranges between 3340 and 3580 m a.s.l. This glacier is mostly in cold thermal conditions and its front hangs over the Fine del Mondo Glacier (Ende der Welt Ferner) underneath.

Mountain permafrost is widespread on Mt. Ortles, according to the permafrost distribution modelled by Boeckli et al. (2012), that indicates 'permafrost in nearly all conditions' above 2600 m for areas with northern exposure, and above 2900 m for areas with southern exposure.

Before the Ortles Project, no specific investigation existed on the air, englacial and permafrost temperatures of this mountain.
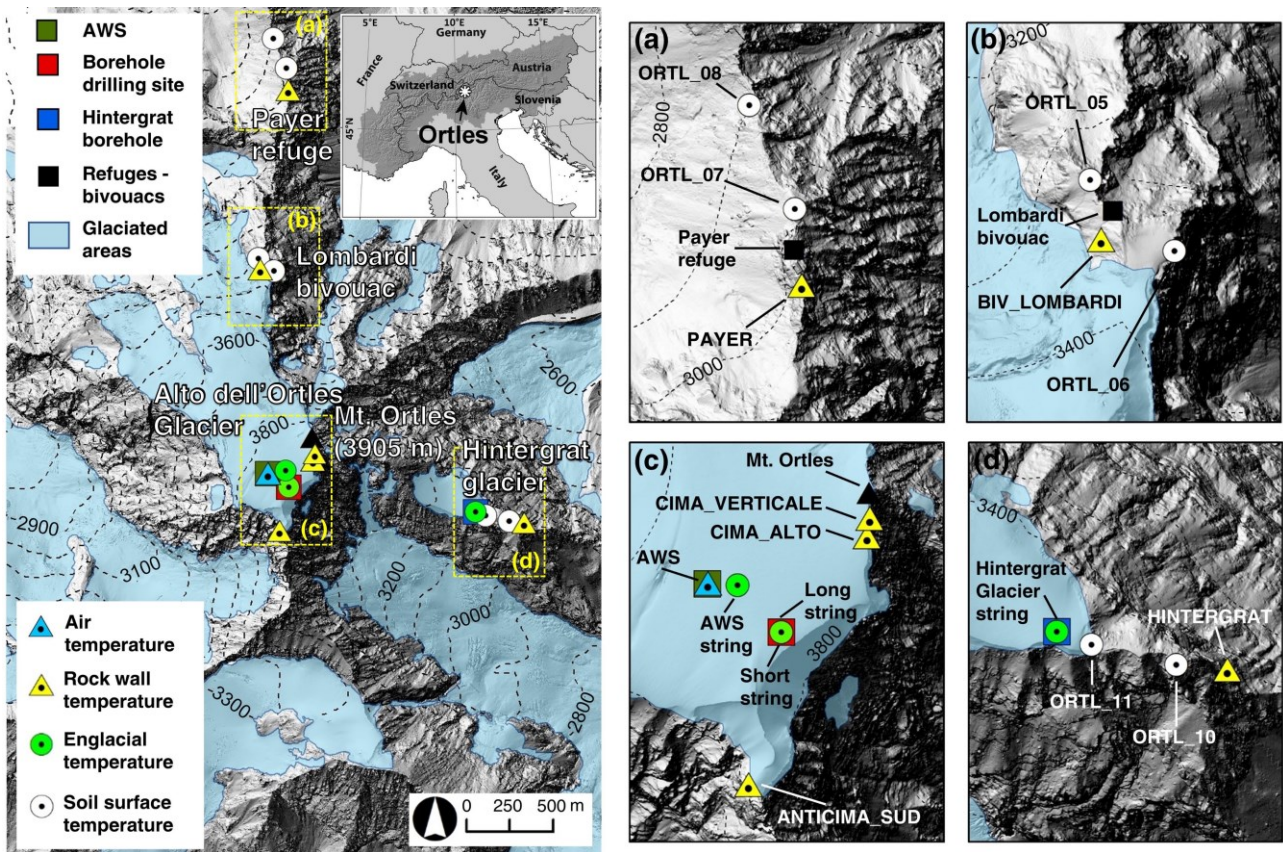
Figure 1. Geographic location of Mt. Ortles and of sites instrumented for air, rock, englacial and soil surface temperature measurements. Close ups of the a) Payer Refuge, b) Lombardi Bivouac, c) Mt. Ortles summit area, and d) Hintergrat ridge are reported in the panes on the right. The background hillshaded DEM (2017 LiDAR survey) is from http://geocatalogo.retecivica.bz.it/.

3. Data description

The temperature datasets presented in this work were obtained by installing stand-alone dataloggers connected to one or several temperature sensors. Due to the remoteness of the study site, dataloggers were powered by lithium or lead-acid batteries, which in the case of the Automatic Weather Station (AWS, Section 3.1) were recharged daily by solar panels. Periodic field visits, mostly performed from June to September, were used for instrumentation maintenance and data download using a laptop. No real-time transmission of data was setup. The dataset is characterised by a good time coverage and a few gaps (Fig. 2), indicating the suitability of the selection of the equipment and field procedures for installation and maintenance. The most significant temporal gaps affect soil surface temperature datasets due to the impossibility of accessing dataloggers in late summer of 2011. Other minor gaps were caused by temporary malfunctions or by damaged equipment, e.g., the rupture

152   of the fan-aspirated radiation shield at the AWS between February and August 2013, which forced us to treat

153   this period as a data gap. We did not undertake gap-filling, in order to keep the data recorded in the field as

154   unchanged as possible.

155   Details of measuring equipment and installations are provided in the following sections. Further details about

156   the instruments are provided in Table 1 and a topographic description of instrumented sites is reported in Table

157   E1, in the Appendix. Figures showing examples of data series for each variable are provided in the following

158   subsections.

159
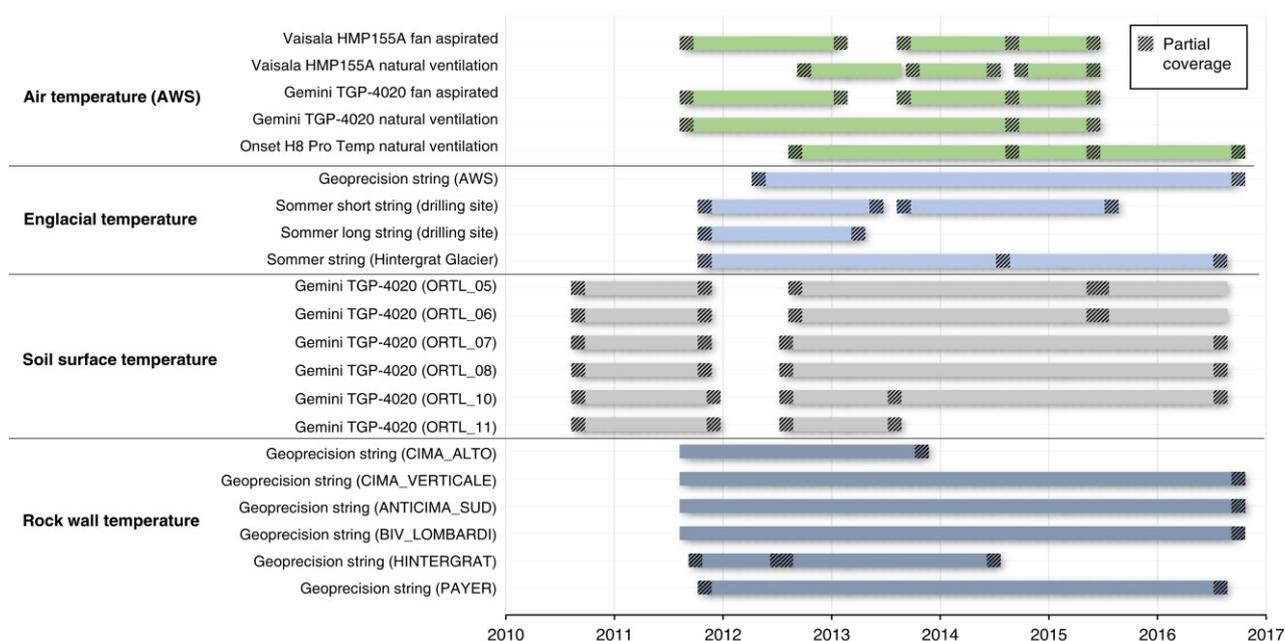
160

161   Figure 2. Monthly coverage of temperature measurements available from 2010 to 2016 on Mt. Ortles. Partial

162   coverage indicates the occurrence of data gaps for specific months.

163

164

165   Table 1. Sensor characteristics, setup and period of operation for air, englacial, soil surface and rock wall

166   temperature measurements on Mt. Ortles.

167

Measured variable	Sensor	Radiation shield	Period of operation		Initial height (m)	Unit	Interval	Integration method and interval	Accuracy
			from	to					
Air temperature data (AWS)									

			Start	End		Unit			Accuracy
Air Temperature	Vaisala HMP155A	R. M. Young 43502 fan-aspirated radiation shield	Sep 2011	Jun 2015	+4	°C	15 min	avg 1 h	±(0.226 - 0.0028·T)°C from -80 to 20°C, ±(0.055 + 0.0057·T)°C from 20 to 60 °C
Air Temperature	Vaisala HMP155A	Campbell Scientific MET 21 radiation shield with natural ventilation	Sep 2012	Jun 2015	+4	°C	15 min	avg 1 h	±(0.226 - 0.0028·T)°C from -80 to 20°C, ±(0.055 + 0.0057·T)°C from 20 to 60 °C
Air Temperature (Backup and comparison)	Gemini TGP-4020	R. M. Young 43502 fan-aspirated radiation shield	Sep 2011	Jun 2015	+4	°C	1 h	avg 1 h	±(0.2 - 0.005·T)°C from -40 to 0°C, ±0.2 °C from 0°C to 40°C
Air Temperature (Backup and comparison)	Gemini TGP-4020	R.M. Young 41303-5 radiation shield with natural ventilation	Sep 2011	Jun 2015	+4	°C	1 h	avg 1 h	±(0.2 - 0.005·T)°C from -40 to 0°C, ±0.2 °C from 0°C to 40°C
Air Temperature (Backup and comparison)	Onset Hobo H8 Pro Temp	Davis 7714 radiation shield with natural ventilation	Sep 2012	Sep 2016	+4	°C	1 h	avg 1 h	±(0.63 - 0.022·T)°C from -40 to 0°C, ±0.63 °C from 0°C to 40°C

Englacial temperature data

			Start	End		Unit			Accuracy
Snow and firn temperature at the AWS site	Geoprecision thermistor string (15 sensors)		Jun 2012	Sep 2016	-0.6 / -1.6 / -2.6 / -3.6 / -4.6 / -5.6 / -6.6 / -7.6 / -8.6 / -9.6 / -10.6 / -11.6 / -12.6 / -13.6 / -14.6	°C	2 h	instant 2 h	±0.5°C from -10°C to +85°C
Englacial temperature at the borehole drilling site (short string)	Sommer thermistor string (11 sensors)		Nov 2011	Aug 2015	0 / -1 / -2 / -3 / -4 / -6 / -8 / -10/ -15 / -20 / -25	°C	1 h	instant 1h	±0.1°C from 0°C to 70°C
Englacial temperature at the borehole drilling site (long string)	Sommer thermistor string (4 sensors)		Nov 2011	Apr 2013	-15 / -35 / -55 / -75	°C	1 h	instant 1h	±0.1°C from 0°C to 70°C
Englacial temperature at the Hintergrat Glacier	Sommer thermistor string (5 sensors)		Nov 2011	Aug 2016	-1.5 / -3.5 / -5.5 / -7.5 / -9.5	°C	1 h	instant 1h	±0.1°C from 0°C to 70°C

Soil surface temperature data

			Start	End		Unit			Accuracy
Soil surface temperature at Lombardi bivouac - ORTL_05	Gemini TGP-4020		Sep 2010	Sep 2016	-0.15	°C	1 h	avg 1h	±(0.2 - 0.005·T)°C from -40 to 0°C, ±0.2 °C from 0°C to 40°C
Soil surface temperature at Lombardi bivouac - ORTL_06	Gemini TGP-4020		Sep 2010	Sep 2016	-0.12	°C	1 h	avg 1h	±(0.2 - 0.005·T)°C from -40 to 0°C, ±0.2 °C from 0°C to 40°C
Soil surface temperature at Payer refuge - ORTL_07	Gemini TGP-4020		Sep 2010	Aug 2016	-0.05	°C	1 h	avg 1h	±(0.2 - 0.005·T)°C from -40 to 0°C, ±0.2 °C from 0°C to 40°C
Soil surface temperature at Payer refuge - ORTL_08	Gemini TGP-4020		Sep 2010	Aug 2016	-0.05	°C	1 h	avg 1h	±(0.2 - 0.005·T)°C from -40 to 0°C, ±0.2 °C from 0°C to 40°C
Soil surface temperature at Hintergrat ridge - ORTL_10	Gemini TGP-4020		Sep 2010	Aug 2016	-0.05	°C	1 h	avg 1h	±(0.2 - 0.005·T)°C from -40 to 0°C, ±0.2 °C from 0°C to 40°C
Soil surface temperature at Hintergrat ridge - ORTL_11	Gemini TGP-4020		Sep 2010	Aug 2013	-0.05	°C	1 h	avg 1h	±(0.2 - 0.005·T)°C from -40 to 0°C, ±0.2 °C from 0°C to 40°C

Rock wall temperature data

Rock wall temperature at Mt. Ortles summit - CIMA_ALTO	Geoprecision thermistor string (3 sensors)	Sep 2011	Nov 2013	-0.10 / -0.30 / -0.55	°C	1 h	instant 1h	±0.5 °C from -30 to -5 °C, ±0.1 °C from -5 to +40 °C
Rock wall temperature Mt. Ortles summit - CIMA_VERTICALE	Geoprecision thermistor string (3 sensors)	Sep 2011	Sep 2016	-0.10 / -0.30 / -0.55	°C	1 h	instant 1h	±0.5 °C from -30 to -5 °C, ±0.1 °C from -5 to +40 °C
Rock wall temperature at Vorgipfel - ANTICIMA_SUD	Geoprecision thermistor string (3 sensors)	Sep 2011	Sep 2016	-0.10 / -0.30 / -0.55	°C	1 h	instant 1h	±0.5 °C from -30 to -5 °C, ±0.1 °C from -5 to +40 °C
Rock wall temperature at Lombardi bivouac - BIV_LOMBARDI	Geoprecision thermistor string (3 sensors)	Sep 2011	Sep 2016	-0.10 / -0.30 / -0.55	°C	1 h	instant 1h	±0.5 °C from -30 to -5 °C, ±0.1 °C from -5 to +40 °C
Rock wall temperature at Hintergrat - HINTERGRAT	Geoprecision thermistor string (3 sensors)	Oct 2011	Aug 2014	-0.10 / -0.30 / -0.55	°C	1 h	instant 1h	±0.5 °C from -30 to -5 °C, ±0.1 °C from -5 to +40 °C
Rock wall temperature at Payer refuge - PAYER	Geoprecision thermistor string (3 sensors)	Nov 2011	Aug 2016	-0.10 / -0.30 / -0.55	°C	1 h	instant 1h	±0.5 °C from -30 to -5 °C, ±0.1 °C from -5 to +40 °C

168

169

170

3.1 Air temperature data

On 30 September 2011 an Automatic Weather Station (AWS, Fig. 3) was installed on the upper accumulation area of Alto dell'Ortles Glacier, at an elevation of 3830 m a.s.l. The AWS was equipped with a Campbell Scientific CR-1000 datalogger, solar panels and sensors for air temperature and relative humidity (Vaisala HMP155A), wind speed and direction (R. M. Young 05103), incoming and outgoing shortwave and longwave radiation (Delta Ohm LP Pyra 05 and LP PIRG 01), and snow depth (Campbell Scientific SR50A). The equipment was supported by an aluminum tower (composed of 2-m modules), anchored in the firn at 2 m depth and supported by wooden boards. After the installation, the tower extended 4 m from the surface. The sensors and solar panels were fixed on top of the tower, whereas the datalogger/battery housing box was fixed at the bottom (Figs. F1 and F2).

181

182

183 Figure 3. The automatic weather station installed in the upper accumulation area of Alto dell'Ortles Glacier.

184 The Mt. Ortles summit (3905 m a.s.l.) is visible in the background.

185

186 The Vaisala HMP155A sensor was installed inside a R. M. Young 43502 fan-aspirated radiation shield. Two

187 standalone Gemini TGP-4020 dataloggers equipped with PB-5003-1 thermistor probes were also installed for

188 comparison and backup purposes, one in the same fan-aspirated radiation shield of the Vaisala HMP155A

189 sensor and one inside a 6-plate R.M. Young 41303-5 radiation shield with natural ventilation. In September

190 2012, we installed an additional HMP155A temperature sensor inside a 15-plate Campbell Scientific MET 21

191 radiation shield with natural ventilation, and an Onset Hobo H8 Pro Temp datalogger housed in an 8-plate

192 Davis 7714 radiation shield with natural ventilation (Figs. F3 and F4). Sensor specifications are reported in

193 Table 1. The Vaisala HMP155A data were recorded as 15-minute mean values, whereas the Gemini TGP-4020

194 dataloggers recorded hourly minimum and maximum temperature, and the Hobo H8 Pro Temp datalogger

195 recorded hourly instantaneous temperature. All the temperature records have been converted into hourly

averages, averaging 15-minute means for the Vaisala HMP155A sensors, minimum and maximum hourly
temperature for the Gemini TGP-4020 dataloggers, and instantaneous temperature at the beginning and at the
end of each hour for the Hobo H8 Pro Temp datalogger, assuming a linear variation of temperature during
each hour.

All the air temperature sensors were installed at the same level (±20 cm). The height of the air temperature
sensors above the glacier surface changed with the snow accumulation over time (mean height = 241 cm, 5th
percentile = 61 cm, 95th percentile = 407 cm). To prevent burial by snow accumulation, the tower was elongated
annually by adding a 2-m module. Figure 4 shows the height of the sensors above the glacier surface, as
reconstructed from the snow depth data and maintenance logs (Table D1).
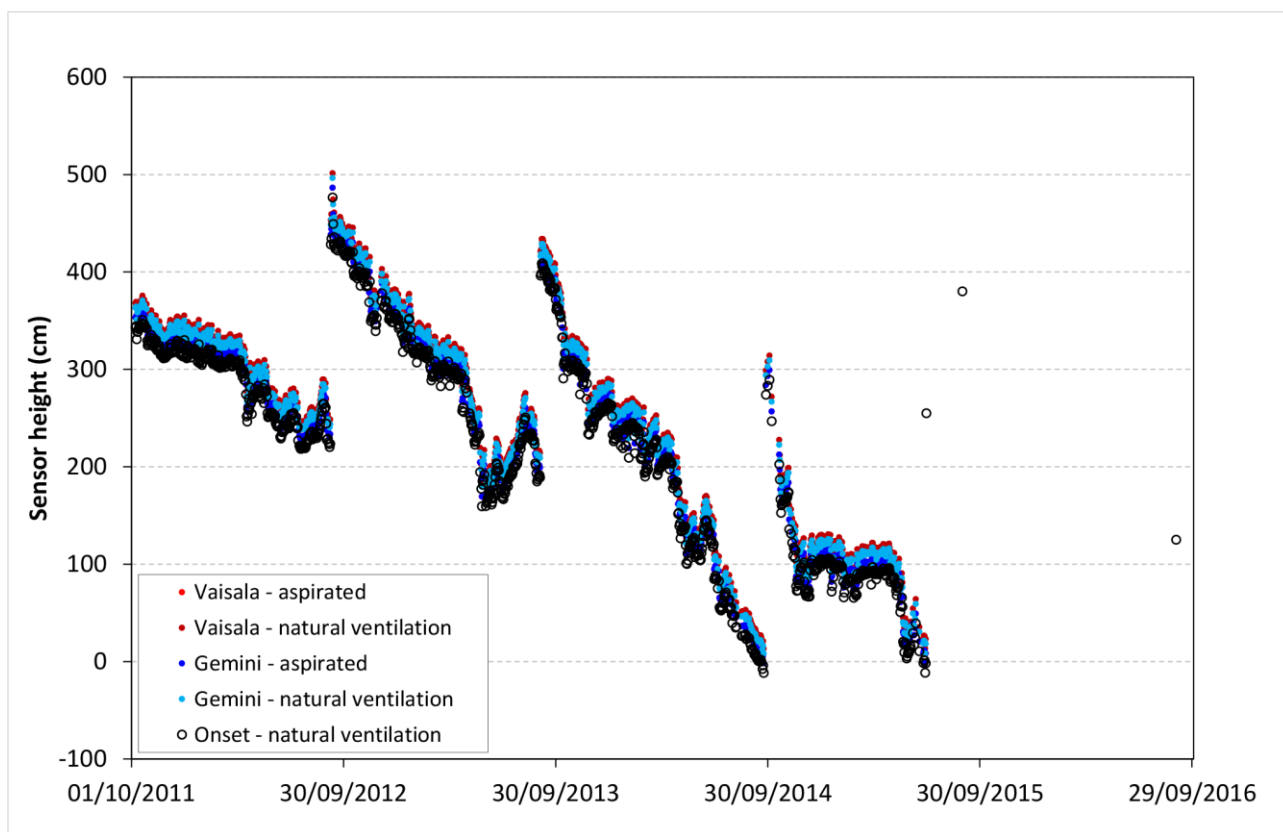
Figure 4. Air temperature sensors height above the snow surface.

Despite the remote and harsh environment, the AWS worked properly without major interruptions. In June
2015 it was removed, but the Hobo H8 Pro Temp logger was left on site and recorded additional 15 months of

data. The main issue linked to the specific environment of installation was ice and snow accretion combined with strong winds, which damaged the fan-aspirated radiations shield in February 2013. The obtained data are shown in Fig. 5.
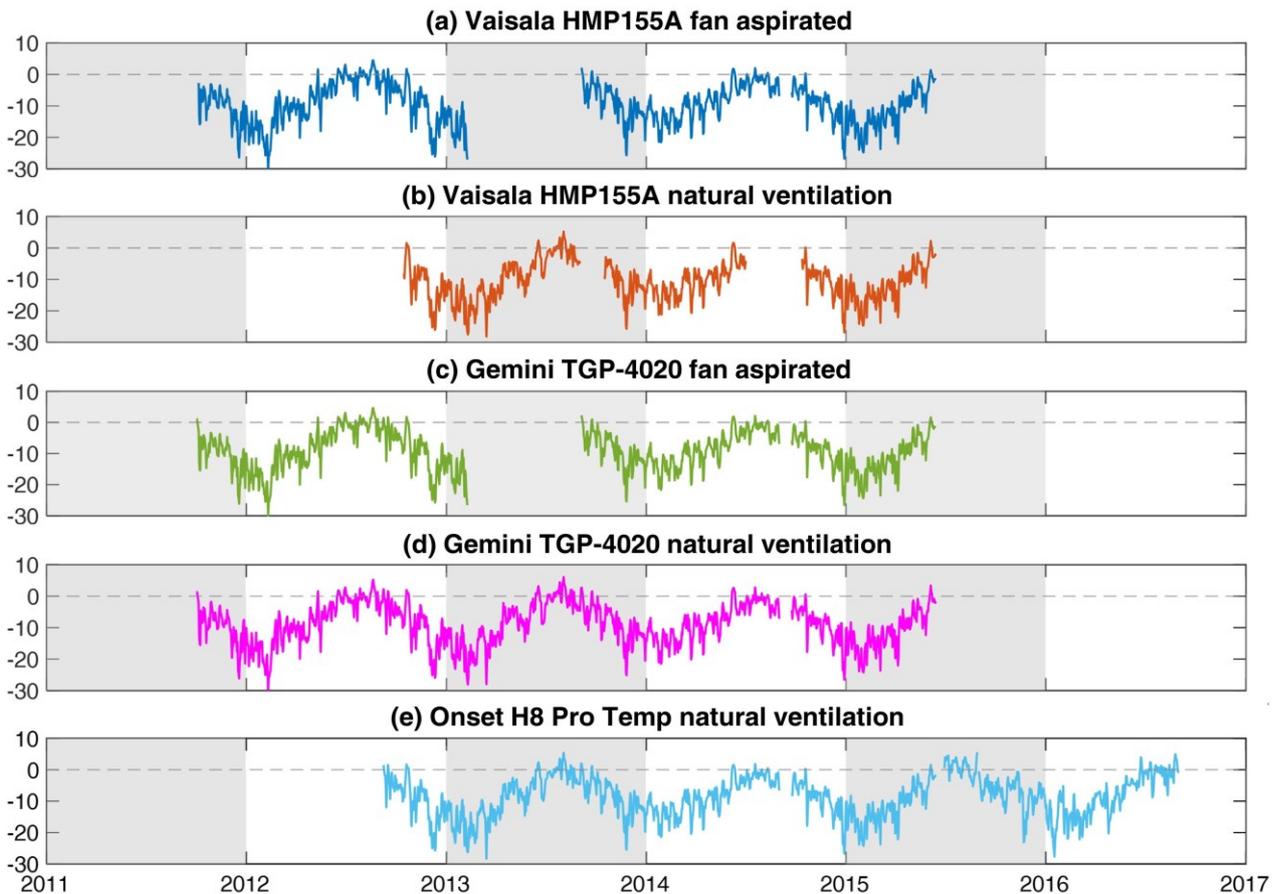
Figure 5. Daily mean air temperature series measured by different sensors installed at the Automatic Weather Station on Mt. Ortles.

3.2 Englacial temperature data

Englacial temperature measurements were collected at three different sites on Mt. Ortles: i) at the AWS site (3830 m), ii) at the borehole drilling site (3859 m), and iii) at the Hintergrat glacier (3476 m). The obtained englacial temperature data are shown in Fig. 6.

3.2.1 Snow and firn temperature data at the AWS site

On the 18th of June 2012 a 20-meter thermistor string manufactured by Geoprecision GmbH (Germany) was installed 10 m east of the AWS (Fig. F1). The thermistor string was composed of a Dallas M-Log5W datalogger, powered by a 3.6 V lithium battery, and connected to 15 digital Dallas temperature sensors spaced one meter from each other. The string was lowered into a 14.6 m hole drilled using a steam ice drill. The initial depth of temperature sensors ranged between 0.6 and 14.6 m, and increased afterwards up to about 6 m due to the accumulation of snow. The logger was housed inside a plastic box on the glacier surface, subsequently buried in the snow. Instantaneous temperature data were recorded with a 2-hour frequency.

The data were retrieved by means of a laptop using a USB dongle connected wireless (radio transmission) to the logger, below the glacier surface. We were able to retrieve temperature data with the logger buried below a maximum of ~6 m of snow and firn. The thermistor string worked properly without interruptions and without requiring maintenance or battery replacement. Sensor specifications are reported in Table 1.

3.2.2 Englacial temperature at the borehole drilling site

The site where the Ortles Project deep ice cores were extracted is a small col (3859 m; 10°32'34", 46°30'25") between the summit of Mt. Ortles and the Anticima Sud/Vorgipfel (3845 m, Figs. 1 and G1). The ice is 75 m thick at this site as indicated by geophysical sensing prospecting and confirmed by ice core drilling operations (Gabrielli et al., 2016). Two thermistor strings were installed in borehole number 3 on the 5th of October 2011, immediately after the completion of the drilling operations (Fig. G3a). The strings were composed of an MDL 8/3 datalogger, manufactured by Sommer GmbH & Co KG (Austria). The logger was connected to 44031 thermistors, manufactured by ThermX (USA).

A first (short) thermistor string was 35 m long, and was equipped with temperature sensors at 0, 1, 2, 3, 4, 6, 8, 10, 15, 20, 25 m (initial depth). The other (long) string was 100 m, with temperature sensors at 15, 35, 55 and 75 m (initial depth). Burial depth of sensor increased over time due to net snow and firn accumulation. Dataloggers and exceeding portions of strings were housed inside a metal box and arranged on a winding system (Fig. G3), making it possible to extend the thermistor strings and to arise the box at the glacier surface periodically. Field maintenance was also required to replace batteries and download the stored data. Instantaneous temperature data were recorded with a 1-hour frequency.

254 The short string worked properly until removal in summer 2015, with the exception of a two-month gap in

255 summer 2013. The long string stopped working in April 2013, possibly due to ice dynamics and deformation

256 of the borehole at a depth below 25-30 m. Sensor specifications are reported in Table 1.

257

258 3.2.3 Englacial temperature at the Hintergrat Glacier

259 On the 14th of October 2011 a thermistor string was installed at 3476 m a.s.l. on top of the Hintergrat Glacier

260 (Fig. G2). The string was manufactured by Sommer GmbH & Co KG (Austria), with the same components as

261 those installed at the ice core drilling site (Section 3.2.2, Fig. G4). It was lowered into a hole drilled using a

262 steam ice drill down to a depth of 9.6 m. We did not reach the glacier bottom at this site. The temperature

263 sensors were placed at 1.5, 3.5, 5.5, 7.5 and 9.5 m below the glacier surface. This lower site is subject to net

264 ablation, therefore in this case the initial depth decreased through time and the sensor at 1.5 m depth came to

265 the surface in summer 2013. After 2013, this sensor's data were consequently discarded.

266

267

268
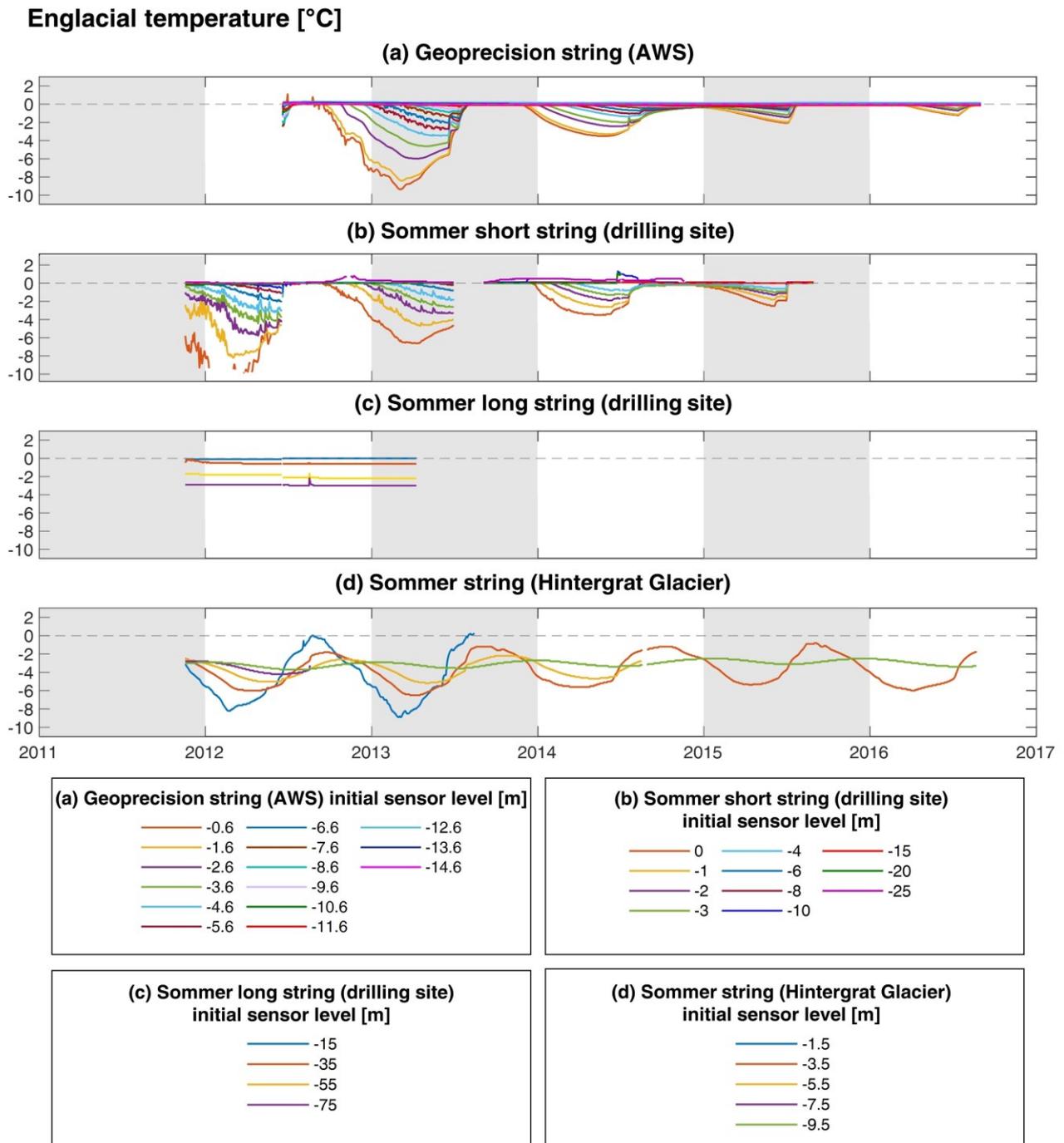
Figure 6. Englacial temperature measured at various sites and various depths on the Alto dell'Ortles Glacier.

3.3 Soil surface temperature data

The thermal regime of the soil surface at six deglaciated sites on Mt. Ortles was monitored using standalone

temperature dataloggers over the period between September 2010 and September 2016. We used Gemini TGP-

4020 dataloggers, powered by 3.6 V lithium batteries, and equipped with PB-5001 probes, which were placed

5-15 cm below the soil surface (Figs. H1 and H2). Mean temperature data were recorded at hourly intervals. Periodic maintenance was required to download the data and replace exhausted batteries.

The monitored sites range in elevation between 2899 and 3466 m a.s.l. The dataloggers were placed in pairs at three main locations (Figs. 1 and H3): refuge Payer (ORTL_07 and ORTL_08), bivouac Lombardi (ORTL_05 and ORTL_06) and Hintergrat ridge (ORTL_10 and ORTL_11).

The data series extend from late summer 2010 to late summer 2016, with a gap between autumn 2011 and late summer 2012 and for ORTL_05 and ORTL_06 also between July and August 2015, due to the impossibility of accessing the dataloggers for maintenance. ORTL_11 was buried under snow and firn after 2013 and has never been recovered. The obtained soil surface temperature data are displayed in Fig. 7.
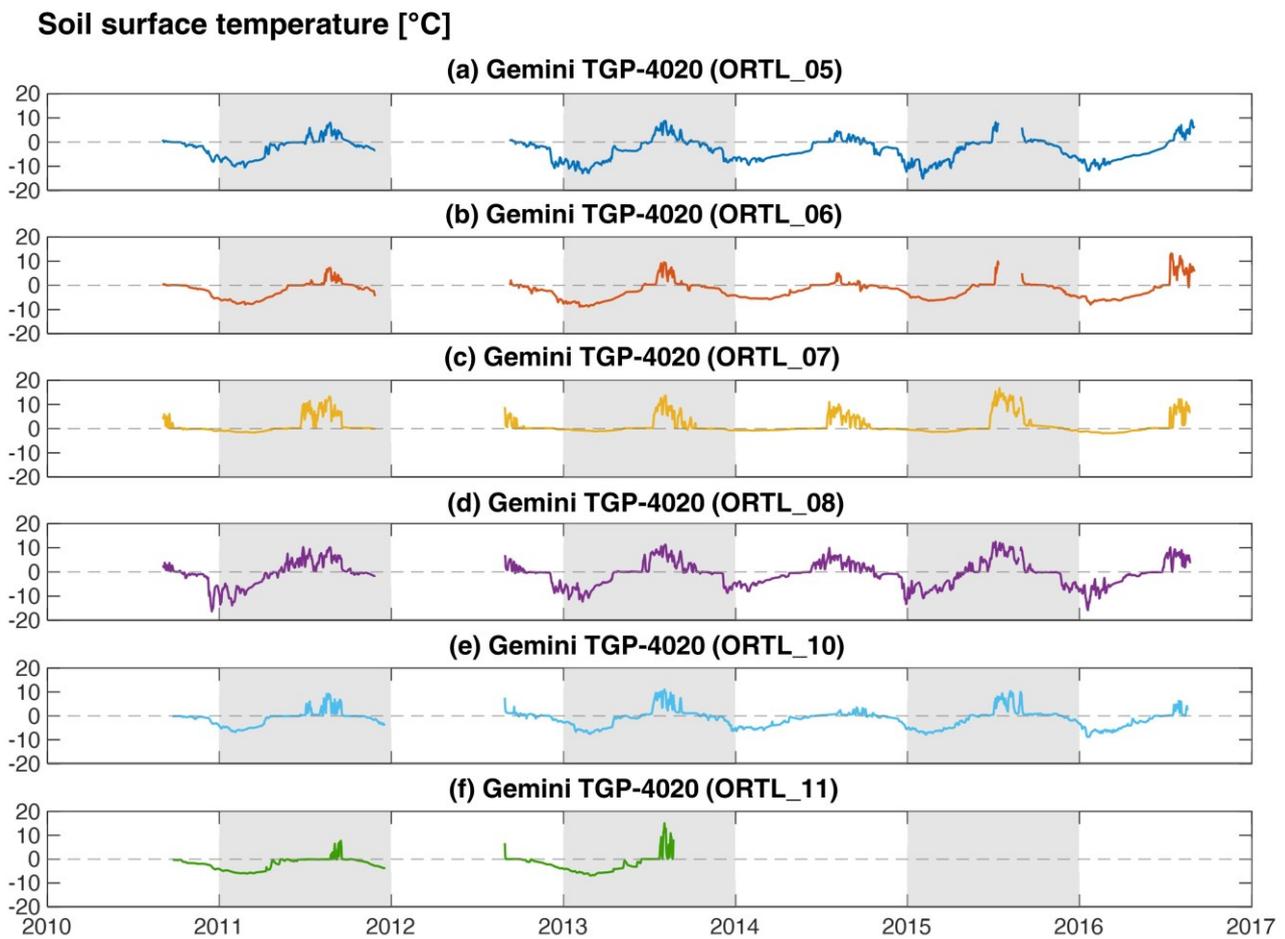
Figure 7. Soil surface temperature data measured at various locations on Mt. Ortles.

291

3.4 Rock wall temperature data

292

The sub-surface temperature of rock walls located at six sites on Mt. Ortles was monitored starting in late

293

summer and autumn 2011 (Fig. 2). Very steep/almost vertical rock walls with different exposures and

294

elevations were selected for monitoring (Figs. 1 and I3, Table E1). Two sites were established next to the Mt.

295

Ortles summit (3900 and 3880 m, facing East), one at the Vorgipfel (3844 m, facing South), one at the

296

Hintergrat (3370 m, facing North-East), one at the bivouac Lombardi (3351, facing West) and one at the refuge

297

Payer (3030 m, facing East).

298

Rock temperature data were acquired using Geoprecision Dallas M-Log5W dataloggers, powered by a 3.6 V

299

lithium battery, and connected to three digital Dallas temperature sensors installed at 0.1, 0.3 and 0.55 m depth,

300

into holes drilled with a hammer drill (Fig. I1). Instantaneous temperature data were stored at hourly intervals

301

and downloaded with a remote connection using a wireless USB dongle and a laptop (Fig. I2).

302

The datalogger placed at the Hintergrat was damaged by hikers in late July 2012 but was repaired in late

303

August 2012. It remained operational until August 2014 when it was removed due to another badly damage.

304

One of the loggers installed at the Mt. Ortles summit ("CIMA_ALTO") stopped working in November 2013

305

due to battery failure while the other dataloggers worked properly until the end of the monitoring period, in

306

late summer 2016. Sensor specifications are reported in Table 1. The obtained rock wall temperature data are

307

displayed in Fig. 8.

308

309

Rock wall temperature [°C]
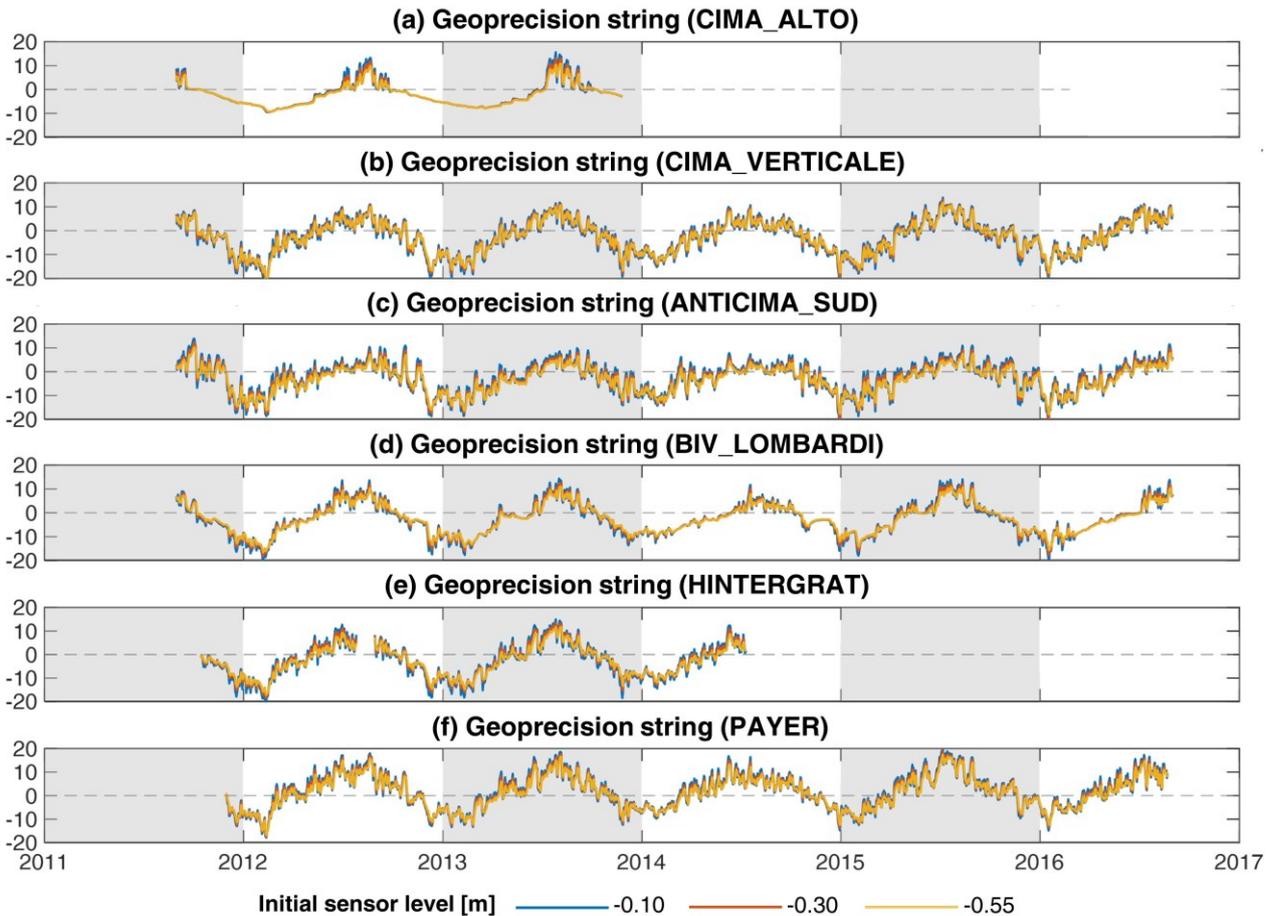
Figure 8. Rock wall temperature measurements at various sites and three depths on Mt. Ortles.

4. Data quality control and assessment

The temperature datasets presented in this work were carefully inspected to detect possible problems affecting raw measurements and to ensure the highest possible accuracy (Table 1). Data quality controls allowed assigning a quality flag to each temperature record, as described in Table B1.

Air temperature sensors were exposed to harsh conditions, without protection from snow, rock or firn/ice as in the case of sensors used to measure the englacial, soil and rock wall temperature. For this reason, the air temperature sensors were subjected to possible damage by strong winds and lightning, ice and snow accretion, and burial by snow in case of abundant snowfall. In addition, they were subjected to the typical issues affecting air temperature measurements, arising from low wind speed and high solar radiation, worsened by high surface albedo, which generally lead to errors due to heating during daytime (WMO, 2021). Sensor drifting should also be taken into account as a potential problem.

324   In order to spot problematic periods we carried out a sensor-by-sensor intercomparison, calculating hourly and

325   daily temperature differences among pairs of sensors, including data from two neighbouring weather stations

326   (Madriccio, 2825 m a.s.l., and Cima Beltovo, 3328 m a.s.l., Weather Service - Autonomous Province of

327   Bozen/Bolzano) for additional confirmation. We compared temperature difference series with maintenance

328   logs, to understand the sources of malfunctions and anomalies, and to assign data quality flags to air

329   temperature series. Data recorded during malfunctions were handled as data gaps and removed from the

330   published series. Anomalies in periods of heavy snowfalls, which caused snow/ice accretion and a rapid

331   decrease of sensor height, are flagged with a specific code (Table B1).

332   Englacial and rock wall temperature were checked in the same way by calculating hourly and daily differences

333   among sensors located at the same site, and checking irregularities (i.e. sudden jumps in temperature

334   differences) in combination with field observations during maintenances. We have detected no malfunctions,

335   but it is possible that after maintenance operations (detailed in Table D1 to D4) a short period of a few hours

336   or a few days was required to reach a new equilibrium at englacial temperature monitoring sites. We have

337   highlighted these maintenance operations with potential impacts on measured temperature using a data quality

338   code, reported in Table B1.

339   Soil surface temperature data displayed no obvious anomalies and were checked in the 'zero-curtain' phase,

340   that is the 0°C plateau during the snowmelt phase. Only ORTL_07 required a correction of measured

341   temperature in 2014 (offset applied = -0.35°C) and 2015 (offset applied = -1.1°C), to correct discrepancies

342   larger than sensor accuracies reported in Table 1. We have highlighted these adjustments with a quality flag in

343   the corresponding data files (Table B1).

344

345   **5. Data availability**

346 The datasets from this study are publicly available at https://doi.org/10.5281/zenodo.7879969 (Carturan et al.,

347 2023). The data files are stored in Microsoft Excel .xlsx format. Detailed information on the file content and

348 structure are reported in the Appendix of this manuscript (Tables A1, B1 and C1).

349

350

351

6. Summary of observations and research outlook

The datasets collected on Mt. Ortles enable description of its thermal state within a time window of six years (2011-2016). This period is long enough to provide a picture of modern average conditions and interannual variability, and it is useful as a baseline for possible future studies aimed at detecting changes and trends in monitored variables.

In the period from 02-10-2011 to 01-09-2016, the mean daily air temperature ranged between -30.1°C (12-02-2012) and 6.1°C (03-08-2013), averaging -8.3°C. These statistics have been extracted from a merged time series, which combines the sensors that have the longest time coverage (Fig. 2), i.e. the GEMINI TGP-4020 with natural ventilation before 15-06-2015 and the ONSET Hobo H8 (natural ventilation) from 15-06-2015. The air temperature reached hourly extremes of -33.3°C (09-02-2012 at 24:00 UTC) and 10.1°C (20-08-2012 at 10:00 UTC). These extremes must be viewed with caution due to the high sensitivity of short-term temperature fluctuations to possible errors, mainly due to low natural ventilation. The aspirated shield installed at the weather station proved subject to damage and malfunction. However, it was operational at the time when the two extreme values were recorded, providing identical minimum temperature of -33.3°C, and a maximum of 8.0°C at 13:00 of 20-08-2012. In the common period of operation (overlaps are shown in Fig. 5), the average difference in mean daily air temperature among pairs of installed sensors did not exceed 0.60°C in absolute value (Table 2).

Table 2. Average difference in mean daily air temperature among pairs of installed sensors (f.a. = fan-aspirated; n.v. = natural ventilation). Column headings represent the first term of the difference calculation.

	Vaisala HMP155A (f.a.)	Vaisala HMP155A (n.v.)	Gemini TGP-4020 (f.a.)	Gemini TGP-4020 (n.v.)	Onset Hobo H8 Pro Temp (n.v.)
Vaisala HMP155A (f.a.)		-0.28	0.11	0.18	-0.02
Vaisala HMP155A (n.v.)			0.41	0.60	0.32
Gemini TGP-4020 (f.a.)				0.08	-0.15

Gemini TGP-4020 (n.v.)				-0.28	

373

374

The mean daily air temperature was above 0°C for 39 days in 2012, 48 in 2013, 15 in 2014, 44 in 2015, and

31 in 2016. These results highlight a significant interannual variability in the length of the melt season at this

high-elevation site. The mean annual air temperature averaged -8.3°C, ranging between -8.6°C in 2012 and

2013, and -7.8°C in 2016 (Table 3).

379

Table 3. Mean annual air temperature recorded at the automatic weather station on Mt. Ortles, with five

different sensors (f.a. = fan-aspirated; n.v. = natural ventilation). The mean temperature is reported only for

years with less than one month missing of data, and is calculated between the 1st of September and the 31st of

August.

384

Sensor	Vaisala HMP155A (f.a.)	Vaisala HMP155A (n.v.)	Gemini TGP-4020 (f.a.)	Gemini TGP-4020 (n.v.)	Onset Hobo H8 Pro Temp (n.v.)	Merged (n.v.)
Year						
2012	-8.9		-8.7	-8.6		-8.6
2013				-8.6	-9.0	-8.6
2014	-8.4		-8.2	-8.1	-8.4	-8.1
2015					-8.6	-8.3
2016					-8.1	-7.8

385

Englacial temperature measurements reveal warm firn and isothermal summer conditions down to a depth of

25 m on the upper part of the Alto dell'Ortles Glacier. The summer was cold (and snowy) enough only in 2014

to preserve below-zero temperature in firn and snow down to a depth of about 15 m at the AWS and 10 m at

the drilling site. On the other hand deep borehole data available until 10/04/2013 confirm that glacier ice below

the firn-ice transition is cold throughout the year, as detected during ice coring operations at the drilling site in

October 2011 (Gabrielli et al. 2012). The ice temperature decreased with depth reaching a minimum of -3°C

at the glacier bed, at 75 m below the surface, and does not change significantly throughout the year.

393   The Hintergrat glacier is also composed of cold ice, which is subject to net surface ablation at the string

394   installation site. Indeed, the sensor at 1.5 m initial depth was exposed at the surface in August 2013. A 1.2 m

395   layer of firn formed in 2014, but underwent complete ablation by the end of the following summer.

396   Soil surface temperature measurements, and in particular the mean annual ground surface temperature

397   (MAGST, Table 4), suggest the existence of permafrost on most of the monitored sites (Guglielmin et al.,

398   2003; Ballantyne, 2018), with the exception of the ORTL07 site which is at 2994 m a.s.l, close to the Payer

399   refuge (Fig. 1).   The results of ORTL_10 and ORTL_11 can be compared to analogous observations

400   (unpublished) carried out in the same period on Mt Vioz (3520 m a.s.l., 14 km south of Mt. Ortles), using the

401   same devices and field techniques at two sites with similar elevation and exposure. On Mt. Vioz the MAGST

402   was -2.1°C for the site with southern exposure and -2.9°C for the site with eastern exposure, indicating slightly

403   colder soil surface thermal conditions.

404

405   Table 4. Mean annual ground surface temperature (MAGST) recorded at six different sites on Mt. Ortles. Site

406   locations are reported in Fig. 1. MAGST is reported only for years with less than one month of missing data,

407   and is calculated between the 1st of September and the 31st of August.

408

Sensor	ORTL_05	ORTL_06	ORTL_07	ORTL_08	ORTL_10	ORTL_11
Year						
2011	-2.6	-2.4	1.3	-1.2	-1.2	-2.4
2012						
2013	-3.5	-2.7	1.1	-1.0	-0.7	-2.1
2014	-3.2	-2.1	0.9	-0.5	-1.5	
2015			1.9	-0.3	-1.0	
2016	-3.4	-1.6	0.7	-1.6	-1.9	

409

410

411

412   Rock wall temperature provided results that are in line with soil surface temperature measurements. The

413   warmest site was close to the Payer refuge, with mean annual rock surface temperature (MARST) above the

414   freezing level (Table 5). All the other monitored rock walls displayed below-freezing MARST and similar

415   behaviour, with the exception of CIMA_ALTO, close to the Mt. Ortles summit, where rock temperature

416   fluctuations appear to be dampened by snow accumulation between September and May (Fig. 8).

The collected data are being analysed for the interpretation of the ice core drilled in the framework of the Ortles Project. In particular, air and englacial temperature data are used for developing and validating a model that aims at reproducing the formation of the isotopic record in snow and firn.

Together with rock wall and soil surface temperature, these datasets represent unique observations at such elevation in the eastern European Alps, and may contribute to the study and understanding of specific aspects of the climatic sensitivity of the alpine cryosphere. For example, they can be used for the development of permafrost distribution and degradation models, air temperature simulations over glacierized areas (including the so-called glacier cooling effect), snow and glacier mass balance models, glacio-hydrological forecasting systems, or dynamic glacier models that take into account the thermal state of glaciers and its variability.

Table 5. Mean annual rock surface temperature (MARST) recorded at six different site on Mt. Ortles. Site locations are reported in Fig. 1. MARST is reported only for years with less than one month of missing data, and is calculated between the 1st of September and the 31st of August.

LOCATION	CIMA_ALTO			CIMA_VERTICALE			ANTICIMA_SUD			BIVACCO_LOMBARDI			HINTERGRAT			PAYER		
Depth (m)	0.10	0.30	0.55	0.10	0.30	0.55	0.10	0.30	0.55	0.10	0.30	0.55	0.10	0.30	0.55	0.10	0.30	0.55
Year																		
2012	-2.1	-2.3	-2.6	-2.6	-2.5	-2.5	-1.8	-2.2	-2.7	-2.4	-2.3	-2.4						
2013	-2.0	-2.3	-2.5	-3.1	-3.1	-3.0	-3.1	-3.5	-3.9	-2.8	-2.7	-2.7	-2.2	-2.1	-2.2	1.4	1.2	0.9
2014				-2.9	-2.8	-2.8	-2.5	-2.8	-3.3	-2.8	-2.7	-2.7				1.8	1.5	1.2
2015				-2.1	-2.1	-2.1	-2.2	-2.6	-3.1	-1.5	-1.4	-1.6				2.7	2.4	2.1
2016				-2.4	-2.3	-2.3	-2.2	-2.5	-3.0	-3.2	-3.1	-3.1				1.9	1.6	1.3

APPENDICES

438 **APPENDIX A: Variables in data files**

439 Table A1. Column names for variables reported in data files.

Variable	Column name
Air temperature (fan-aspirated Vaisala HMP155A)	Air_T_HMP_Asp
Air temperature (natural-ventilation Vaisala HMP155A)	Air_T_HMP_Nat
Air temperature (fan-aspirated Gemini TGP-4020)	Air_T_TGP_Asp
Air temperature (natural-ventilation Gemini TGP-4020)	Air_T_TGP_Nat
Air temperature (natural-ventilation Onset Hobo H8 Pro Temp)	Air_T_H8_Nat
Englacial temperature at the AWS site	AWS_En (depth m)
Englacial temperature at the borehole drilling site (short string)	BH_En_SS (depth m)
Englacial temperature at the borehole drilling site (long string)	BH_En_LS (depth m)
Englacial temperature at the Hintergrat Glacier	HG_En (depth m)
Soil surface temperature at bivouac Lombardi - ORTL_05	GST_ORTL05
Soil surface temperature at bivouac Lombardi - ORTL_06	GST_ORTL06
Soil surface temperature at refuge Payer - ORTL_07	GST_ORTL07
Soil surface temperature at refuge Payer - ORTL_08	GST_ORTL08
Soil surface temperature at Hintergrat ridge - ORTL_10	GST_ORTL10
Soil surface temperature at Hintergrat ridge - ORTL_11	GST_ORTL11
Rock wall temperature at Mt. Ortles summit - CIMA_ALTO	Rw_ALTO (depth m)
Rock wall temperature Mt. Ortles summit - CIMA_VERTICALE	Rw_VERTICALE (depth m)
Rock wall temperature at Vorgipfel - ANTICIMA_SUD	Rw_ANTICIMA (depth m)
Rock wall temperature at bivouac Lombardi - BIV_LOMBARDI	Rw_LOMBARDI (depth m)
Rock wall temperature at Hintergrat - HINTERGRAT	Rw_HINTERGRAT (depth m)
Rock wall temperature at refuge Payer - PAYER	Rw_PAYER (depth m)

440

441

APPENDIX B: Quality flags for data files

Table B1. Quality code flags reported in data files, their meaning and explanations.

Quality code flag ("_Fl" inflection in column names)	Meaning	Explanation
1	Good data	No issues detected during quality checks
0	No data	Data missing or removed (malfunctioning, physically implausible, sensor/device damaged, sensor underneath snow)
2	Maintenance	Data are affected by field maintenance of instrumentation
3	Ice/snow accretion	The air temperature data are affected by ice or snow accretion
4	Small height of the sensor	The air temperature sensor is less than 1 m above the snow surface
5 (offset)	Sensor offset	Offset applied to correct soil surface temperature data, based on the zero-curtain phase during snow melt (offset value in brackets)

444

445

446

APPENDIX C: Data files structure

Table C1. Structure of data files. For sensors at different depth below the surface, the depth in m is reported

after the variable name, in brackets.

Date and hour (UTC)	Variable name (depth m)	Quality flag code
DD/MM/YYYY HH:MM	value	code

450
451
452
453

454
455

APPENDIX D: Maintenance logs

Table D1. Field operations and maintenance for the air temperature sensors mounted at the AWS on Mt. Ortles.

Date	Field operations
01/10/2011	AWS setup and datalogger launch
18/06/2012	Datalogger download, check of sensor status and functioning
07/09/2012	Datalogger download, check of sensor status and functioning, 2 m increase in height of support tower, installation of two additional sensors (Vaisala HMP155A with natural ventilation, and Onset Hobo H8 Pro Temp)
01/07/2013	Datalogger download, check of sensor status and functioning. The fan-aspirated radiation shield was found damaged and not working

Date	Field operations
03/09/2013	Datalogger download, check of sensor status and functioning, 2 m increase in height of support tower. The fan-aspirated radiation shield was repaired and resumed working properly
03/07/2014	Datalogger download, check of sensor status and functioning
23/09/2014	2 m elongation of support tower. Sensors have been partially buried by snow between 2 and 23/09/2014
29/06/2015	Datalogger download, check of sensor status and functioning. Support tower lengthened by 2 m. Sensors have been partially buried by snow between 15 and 29/06/2015. Removal of all sensors except the Onset Hobo H8 Pro Temp
31/08/2015	Onset Hobo H8 Pro Temp download, check of sensor status and functioning
02/09/2016	Onset Hobo H8 Pro Temp download, check of sensor status and functioning. Sensor removed

458

459

460   Table D2. Field operations and maintenance for the englacial temperature sensors installed on Mt. Ortles.

Date	Field operations
17/11/2011	Installation and launch of the Sommer thermistor strings at the borehole drilling site and at the Hintergrat Glacier.
18/06/2012	Installation and launch of the Geoprecision thermistor string at the AWS site. Download and maintenance (battery replacement) of the Sommer thermistor strings at the borehole drilling site
28/08/2012	Download and maintenance (battery replacement) of the Sommer thermistor string at the Hintergrat Glacier. Sensor at 7.5 m initial depth stopped working on 18/08/2012
07/09/2012	Download of the Geoprecision thermistor string at the AWS site. Download and maintenance (battery replacement) of the Sommer thermistor strings at the borehole drilling site
01/07/2013	Download of the Geoprecision thermistor string at the AWS site. Download and maintenance (battery replacement, logger raised to the surface) of the Sommer thermistor strings at the borehole drilling site
23/08/2013	Download and maintenance (battery replacement) of the Sommer thermistor string at the Hintergrat Glacier. The sensor at 1.5 m initial depth was above the glacier surface
03/09/2013	Download of the Geoprecision thermistor string at the AWS site. Download and maintenance (battery replacement) of the Sommer thermistor strings at the borehole drilling site. Long string stopped working on 10/04/2013
03/07/2014	Download and maintenance (battery replacement, logger replacement) of the short Sommer thermistor string at borehole drilling site. Removal of the datalogger of the long Sommer thermistor string at borehole drilling site (no longer working).
28/08/2014	Download and maintenance (battery replacement) of the Sommer thermistor string at the Hintergrat Glacier. Sensor at 5.5 m initial depth stopped working on 17/08/2014
23/09/2014	Download and maintenance (battery replacement, logger raised to the surface) of the short Sommer thermistor string at the borehole drilling site
18/10/2014	Download of the Geoprecision thermistor string at the AWS site
29/06/2015	Download of the Geoprecision thermistor string at the AWS site
27/08/2015	Download and maintenance (battery replacement) of the Sommer thermistor string at the Hintergrat Glacier
31/08/2015	Download and removal of the short Sommer thermistor string at the borehole drilling site
23/08/2016	Download and removal of the Sommer thermistor string at the Hintergrat Glacier
02/09/2016	Download of the Geoprecision thermistor string at the AWS site

461

462

463   Table D3. Field operations and maintenance for the soil surface temperature sensors installed on Mt. Ortles.

Date	Field operations
02/09/2010	Installation and launch of the ORTL_05, ORTL_06, ORTL_07 and ORTL_08 Gemini TGP-4020
23/09/2010	Installation and launch of the ORTL_10 and ORTL_11 Gemini TGP-4020
28/08/2012	Download and maintenance (battery replacement, logger re-launch) at the ORTL_07, ORTL_08, ORTL_10 and ORTL_11
07/09/2012	Download and maintenance (battery replacement, logger re-launch) at the ORTL_05 and ORTL_06
23/08/2013	Download and maintenance (battery replacement, logger re-launch) at the ORTL_07, ORTL_08, ORTL_10 and ORTL_11
03/09/2013	Download and maintenance (battery replacement, logger re-launch) at the ORTL_05 and ORTL_06
28/08/2014	Download and maintenance (battery replacement, logger re-launch) at the ORTL_07, ORTL_08 and ORTL_10. ORTL_05, ORTL_06 and ORTL_11 not found, buried by snow
27/08/2015	Download and maintenance (battery replacement, logger re-launch) at the ORTL_07, ORTL_08 and ORTL_10
31/08/2015	Download and maintenance (battery replacement, logger re-launch) at the ORTL_05 and ORTL_06
23/08/2016	Download and removal of the ORTL_07, ORTL_08 and ORTL_10
02/09/2016	Download and removal of the ORTL_05 and ORTL_06

464
465

466   Table D4. Field operations and maintenance for the rock wall temperature sensors installed on Mt. Ortles.

Date	Field operations
30/08/2011	Installation and launch of the Geoprecision thermistor strings at CIMA_ALTO, CIMA_VERTICALE, ANTICIMA_SUD, BIV_LOMBARDI
14/10/2011	Installation and launch of the Geoprecision thermistor string at HINTERGRAT
28/11/2011	Installation and launch of the Geoprecision thermistor string at PAYER
28/08/2012	Download of thermistor strings at HINTERGRAT and PAYER. Repair of the Geoprecision thermistor string at HINTERGRAT
07/09/2012	Download of thermistor strings at CIMA_ALTO, CIMA_VERTICALE, ANTICIMA_SUD, BIV_LOMBARDI
23/08/2013	Download of thermistor strings at HINTERGRAT and PAYER
03/09/2013	Download of thermistor strings at CIMA_ALTO, CIMA_VERTICALE, ANTICIMA_SUD, BIV_LOMBARDI
28/08/2014	Download of thermistor string at PAYER
01/09/2014	Download of thermistor strings at HINTERGRAT, damaged, removed
27/08/2015	Download of thermistor string at PAYER
31/08/2015	Download of thermistor strings at CIMA_ALTO, CIMA_VERTICALE, ANTICIMA_SUD, BIV_LOMBARDI. CIMA_ALTO damaged, removed
23/08/2016	Download and removal of the thermistor string at PAYER
02/09/2016	Download and removal of the thermistor strings at CIMA_VERTICALE, ANTICIMA_SUD, BIV_LOMBARDI

467
468

469 **APPENDIX E: Characteristics of measurement sites**

470 Table E1. Topographic and geomorphological characteristics of sites instrumented for temperature

471 measurements.

Measured variable	Elevation (m a.s.l.)	East coordinate UTM WGS84 (m)	North coordinate UTM WGS84 (m)	Aspect	Slope (degrees)	Site description
Air Temperature (automatic weather station)	3830	618254	5151614	NW	11	Upper accumulation area of Alto dell'Ortles Glacier
Snow and firn temperature at the AWS site	3830	618260	5151619	NW	11	Upper accumulation area of Alto dell'Ortles Glacier
Englacial temperature at the borehole drilling site (short and long strings)	3859	618373	5151536	W	7	Upper accumulation area of Alto dell'Ortles Glacier
Englacial temperature at the Hintergrat Glacier	3476	619435	5151395	N	12	Hintergrat Glacier
Soil surface temperature at Lombardi bivouac - ORTL_05	3351	618202	5152846	SW	7	Northern ridge of Mt. Ortles, bedrock covered by a thin layer of debris (fine gravel, sand)
Soil surface temperature at Lombardi bivouac - ORTL_06	3371	618284	5152772	N	22	Northern ridge of Mt. Ortles, recently deglaciated bedrock covered by a discontinuous layer of loose debris (fine gravel, sand)
Soil surface temperature at Payer - refuge ORTL_07	2994	618361	5153936	N	22	Northern ridge of Mt. Ortles, bedrock covered by a thick layer of debris (pebbles, gravel, sand) with sparse vegetation
Soil surface temperature at Payer - refuge ORTL_08	2899	618287	5154105	W	36	Northern ridge of Mt. Ortles, bedrock covered by coarse debris with isolated areas of thinner debris (fine sand and silt).
Soil surface temperature at Hintergrat ridge ORTL_10	3460	619628	5151341	S	22	Eastern ridge of Mt. Ortles, bedrock covered by a layer of debris (fine gravel, sand).
Soil surface temperature at Hintergrat ridge ORTL_11	3466	619491	5151374	SE	11	Eastern ridge of Mt. Ortles, bedrock covered by a thin layer of coarse debris (gravel, sand), close to the edge of the Hintergrat Glacier
Rock wall temperature at Mt. Ortles summit - CIMA_ALTO	3900	618512	5151691	E	70	70 m south of Mt. Ortles summit (3905 m), in a sub-vertical rock face about 30 m below the crest edge
Rock wall temperature Mt. Ortles summit - CIMA_VERTICALE	3880	618512	5151691	E	90	70 m south of Mt. Ortles summit (3905 m), in a vertical rock face about 50 m below the ridge, 20 m below CIMA_ALTO
Rock wall temperature at Vorgipfel - ANTICIMA_SUD	3810	618327	5151269	S	90	Vertical rock face, about 10 m below the upper rock wall edge
Rock wall temperature at Lombardi bivouac - BIV_LOMBARDI	3351	618213	5152784	W	70	Northern ridge of Mt. Ortles, sub-vertical rock wall, about 30 m below the crest edge
Rock wall temperature at Hintergrat - HINTERGRAT	3370	619710	5151334	NE	90	Eastern ridge of Mt. Ortles, vertical rock wall, about 10 m below the crest edge
Rock wall temperature at Payer refuge - PAYER	3030	618372	5153812	SE	90	Northern ridge of Mt. Ortles, vertical rock wall, about 20 m below the crest edge

472

APPENDIX F: Description of the measuring equipment for air temperature

474

475

476   Figure F1. The automatic weather station (AWS) installed on Mt. Ortles, whose summit is visible in the

477   background. The stake behind the weather station indicates the site of the Geoprecision thermistor string. Photo

478   taken on 7 September 2012, after the lengthening of the support tower.

479

480

Figure F2. The wooden boards placed at the bottom of the support aluminum tower, at 2 m depth in the firn,
during the AWS installation. Photo taken on 30 September 2011.
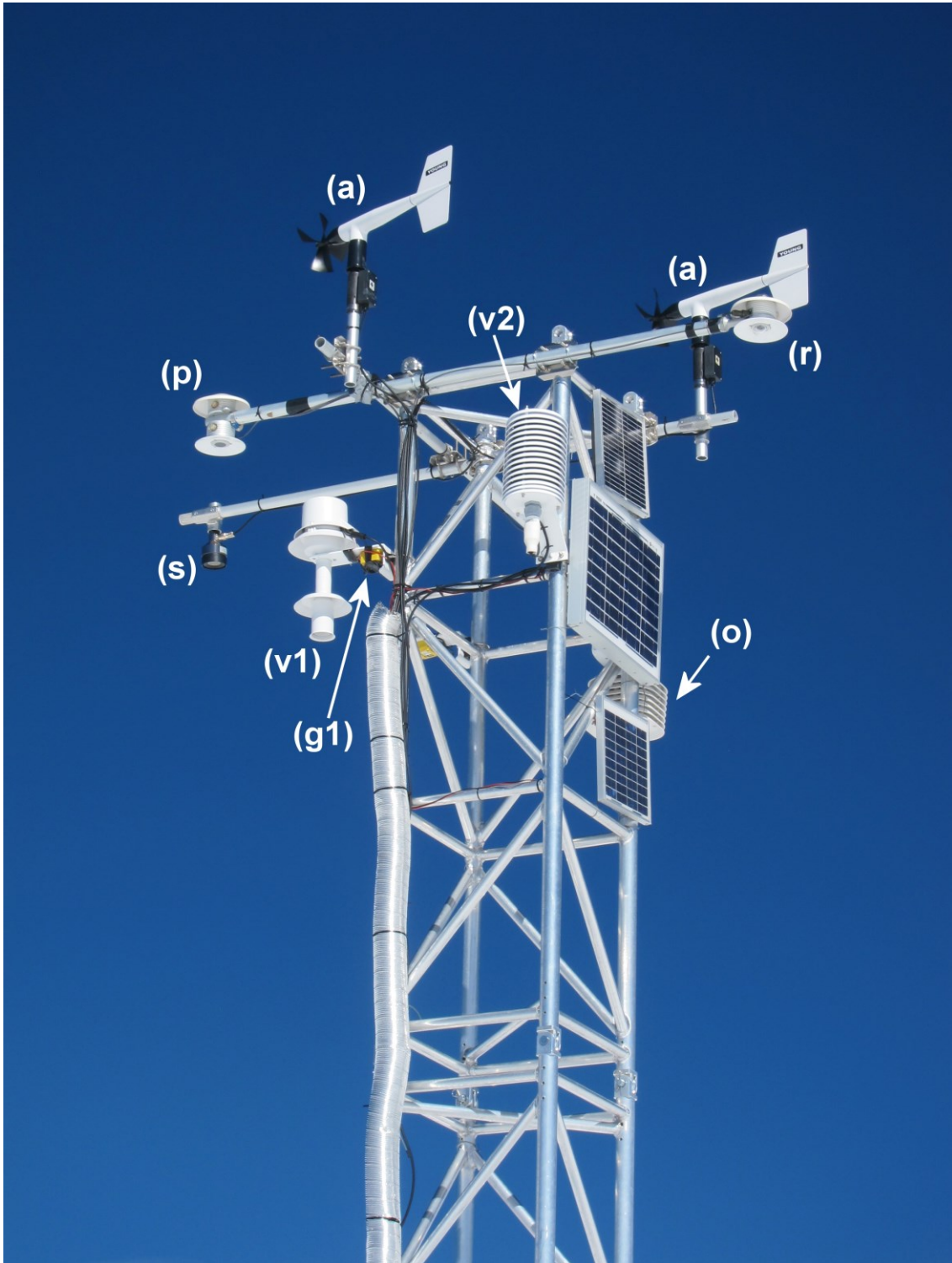
483

484 Figure F3. Detail of the AWS seen from the west: a) R. M. Young 05103 anemometers, p) Delta Ohm LP

485 PIRG 01 pyrgeometers, r) Delta Ohm LP Pyra 05 radiometers, s) Campbell Scientific SR50A snow depth

486 sensors, v1) Vaisala HMP155A inside the R. M. Young 43502 fan-aspirated radiation shield, g1) Gemini TGP-

487 4020 datalogger inside the R. M. Young 43502 fan-aspirated radiation shield, v2) Vaisala HMP155A inside

488 the 15-plates Campbell Scientific MET 21 radiation shield with natural ventilation, o) Onset Hobo H8 Pro

489   Temp datalogger inside the 8-plates Davis 7714 radiation shield with natural ventilation. Photo taken on 7

490   September 2012.

491

492
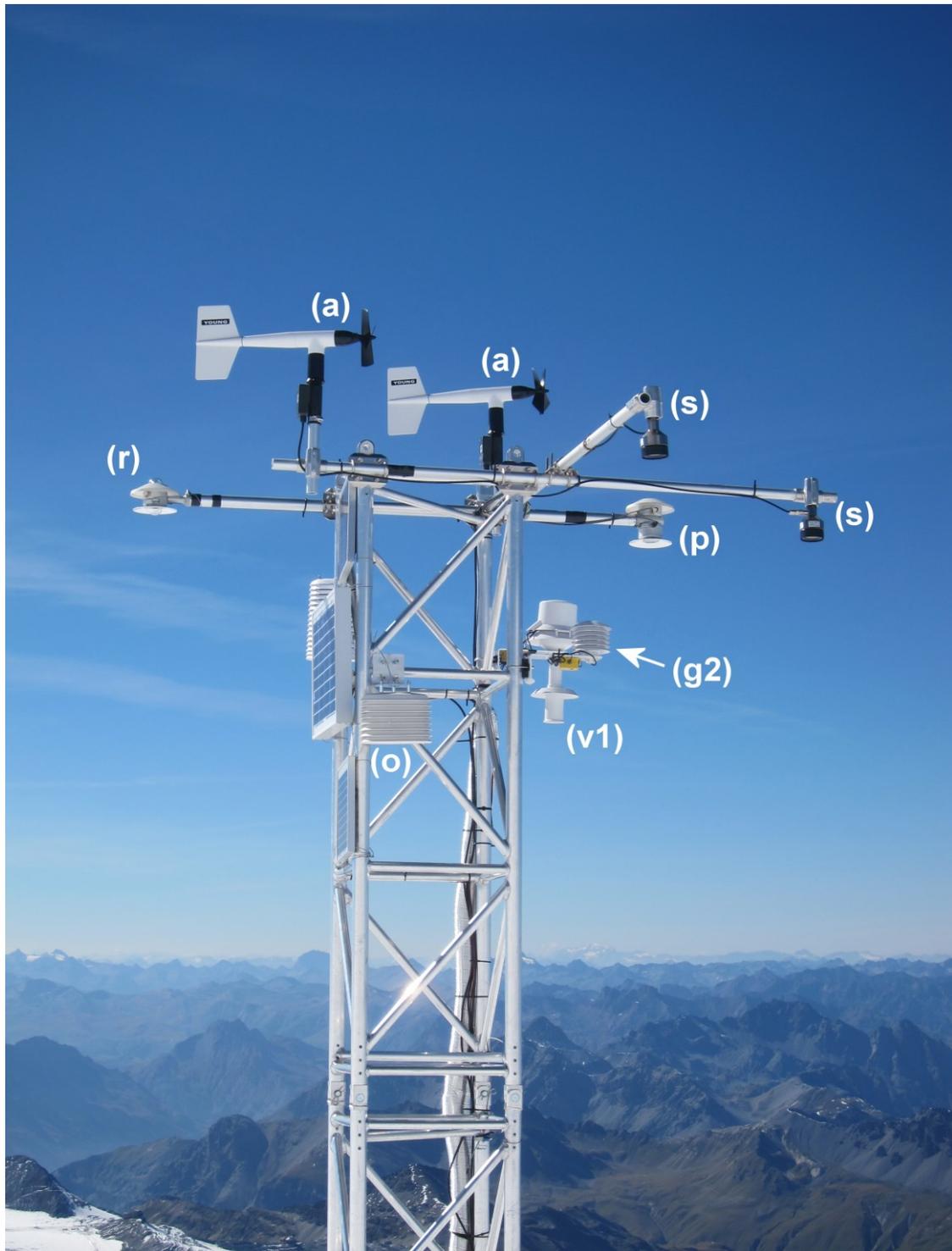
493

494   Figure F4. Detail of the AWS seen from the east: a) R. M. Young 05103 anemometers, p) Delta Ohm LP PIRG

495   01 pyrgeometers, r) Delta Ohm LP Pyra 05 radiometers, s) Campbell Scientific SR50A snow depth sensors,

v1) Vaisala HMP155A inside the R. M. Young 43502 fan-aspirated radiation shield, g2) Gemini TGP-4020 datalogger inside the 6-plates R.M. Young 41303-5 radiation shield with natural ventilation, o) Onset Hobo H8 Pro Temp datalogger inside the 8-plates Davis 7714 radiation shield with natural ventilation. Photo taken on 7 September 2012.

APPENDIX G: Description of the measuring equipment for englacial temperature

Figure G1. The drilling site seen from the summit of Mt. Ortles. The Vorgipfel-Anticima Sud is visible in the background. Photo taken on 1 October 2011 during the ice drilling operations, and before setting up the drilling site thermistor strings for englacial temperature measurements.

511

512

513

514

515

516

517

518 Figure G2. The Hintergrat Glacier seen from the south east (aerial photo taken on 28 August 2012). The black

519 asterisk indicates the location of the borehole equipped with the thermistor string.

520

521

522

523

524

525

526

527

528
529

530
531
532 Figure G3. a) Lowering of a thermistor string into the borehole n. 3 at the drilling site. b) The winding systems

533 of the two thermistor strings installed at the drilling site. c) The two metal boxes containing the thermistor

534 string data loggers and the batteries. d) Final arrangement of the box housing the winding systems and the data

535 loggers. The summit of Mt. Ortles is visible in the background. Photos taken on 17 November 2011.

536

537

538

539

540

541
542
543
544

545
546
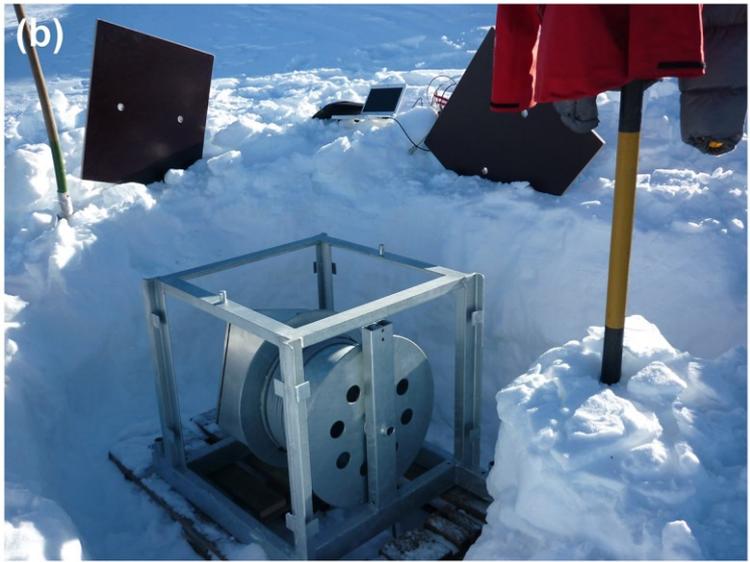
547

548   Figure G4. a) Borehole drilling at the Hintergrat Glacier using a steam ice drill. b) The box containing the

549   winding system, the thermistor string data logger and the batteries. c) Final arrangement of the box housing

550   the winding systems and the data logger. Photos taken on 17 November 2011 and 27 August 2015.

551

552   **APPENDIX H: Description of the measuring equipment for soil surface temperature**

553

554

555   Figure H1. The soil surface temperature datalogger (Gemini TGP-4020) installed at the ORTL_05 site, close

556   to the Lombardi bivouac. The white ellipse indicates the PB-5001 external probe placed underneath the debris

557   surface. Photo taken on 2 September 2010.

558

559

560

561

562 Figure H2. Data download and logger maintenance at the ORTL_10 soil surface temperature site on 28

563 August 2012.

564

565

566

567

568
569
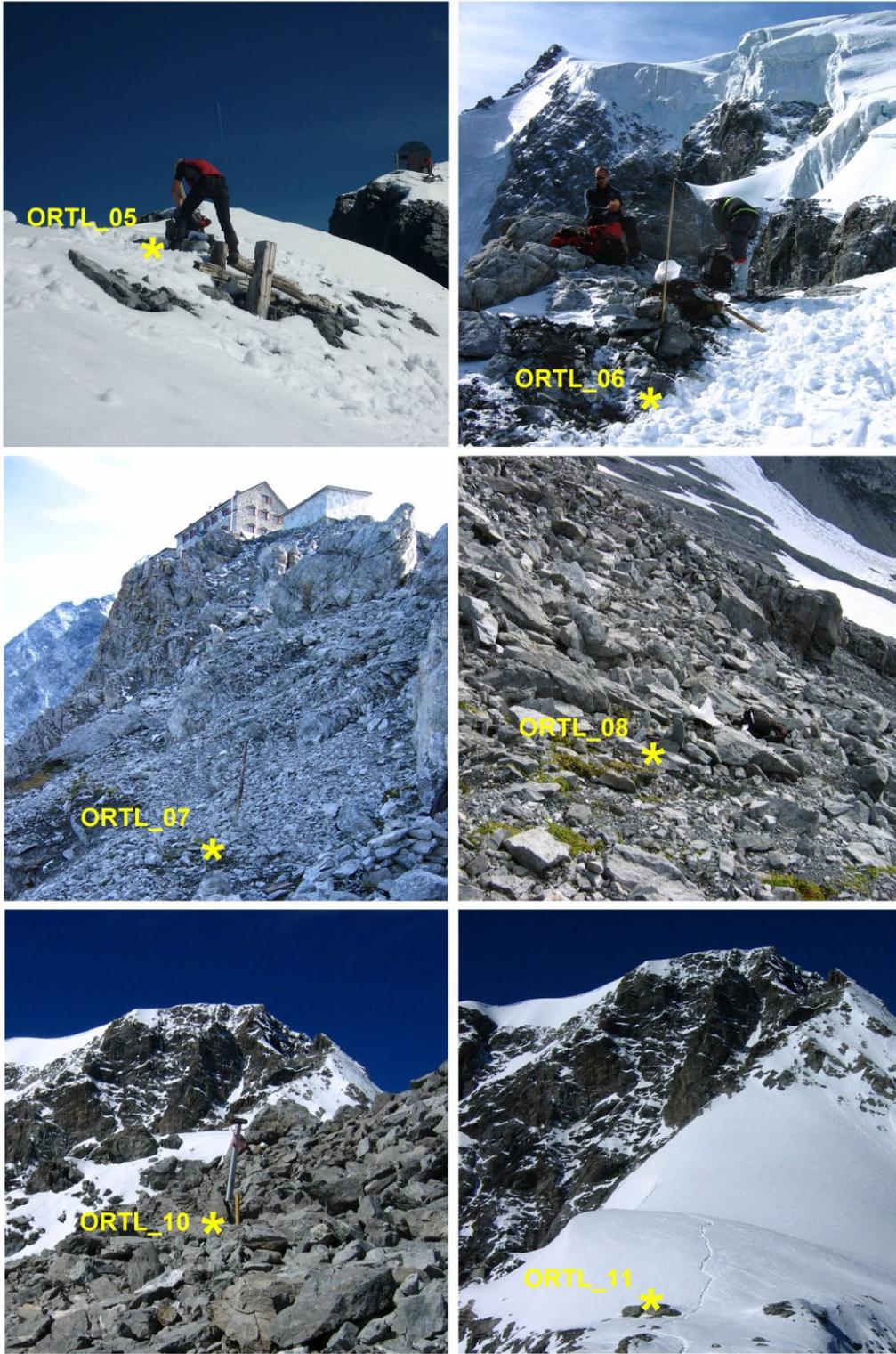
570
571
Figure H3. Location of the six sites equipped with dataloggers for soil surface temperature measurement on

Mt. Ortles.

574

575

576

577 **APPENDIX I: Description of the measuring equipment for rock wall temperature**

578
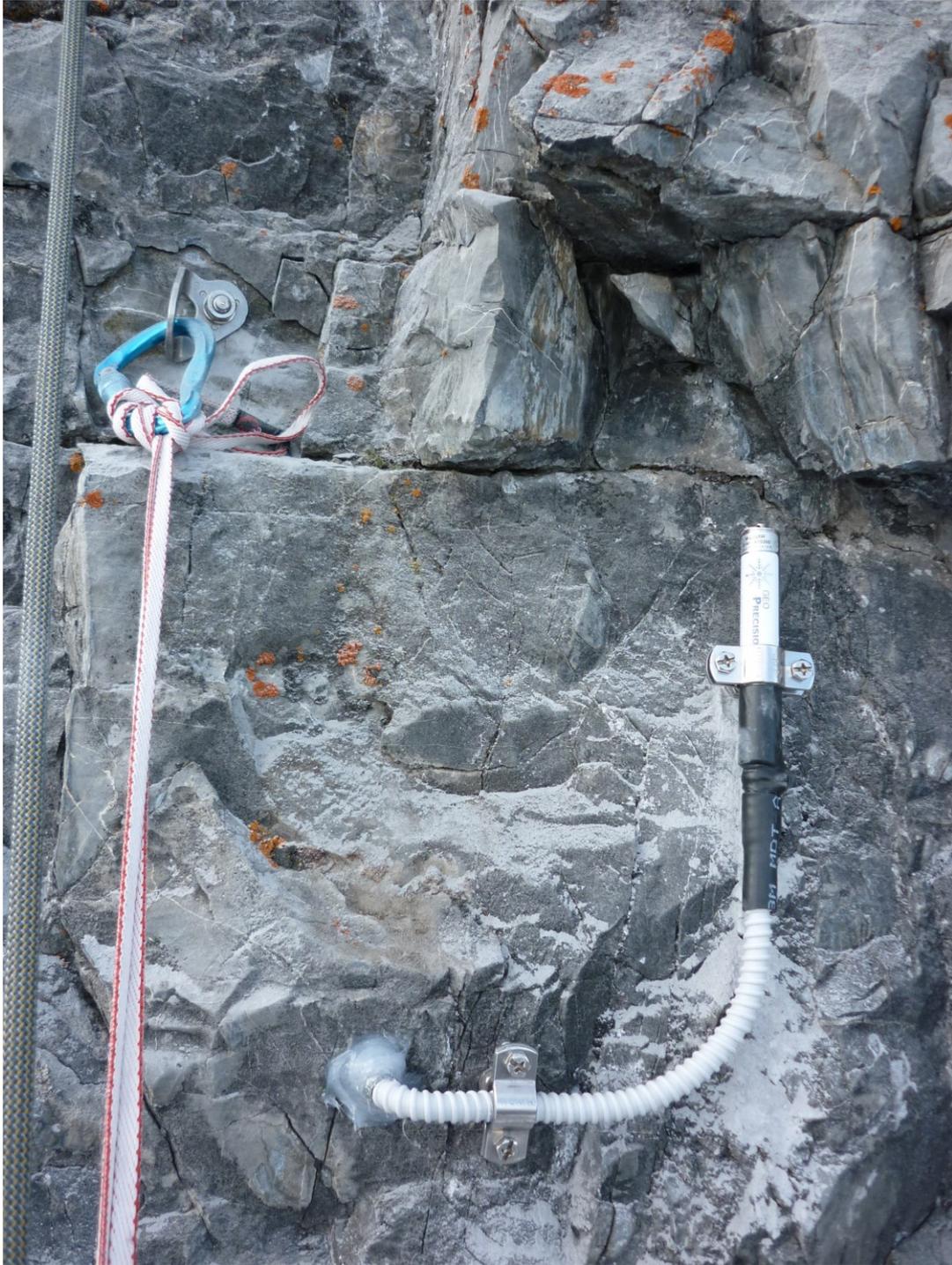
579

580 Figure I1. The rock wall temperature datalogger (Geoprecision thermistor string) installed close to the Payer

581 refuge. The datalogger is anchored to the rock wall and is connected to three temperature sensors placed at 0.1,

582 0.3 and 0.55 m depth inside a horizontal hole drilled in the rock wall. Photo taken on 28 November 2011.

583

584
585

586   Figure I2. Launching of the CIMA ALTO data logger. A wireless USB dongle secures the wireless

587   connection to the laptop used for launching the logger and for downloading the temperature data. Photo

588   taken on 30 August 2011.

589

590

591
592

Figure I3. Location of the six sites equipped with data loggers for rock wall temperature measurement on Mt.

Ortles (BIV_LOMBARDI and HINTERGRAT from Google Earth Pro 7.3 (2022)).

595

596

Acknowledgements

This work is a contribution to the Ortles Project, a program supported by two NSF awards no. 1060115 & no. 1461422 to The Ohio State University and by the Ripartizione Protezione Antincendi e Civile of the Autonomous province of Bolzano in collaboration with the Ripartizione Opere idrauliche e Ripartizione Foreste of the Autonomous province of Bolzano and the Stelvio National Park. This is Ortles Project publication 11 (www.ortles.org). The research was funded by the Italian MIUR Project (PRIN 2010-11), "Response of morphoclimatic system dynamics to global changes and related geomorphological hazards" (local and national coordinators G. Dalla Fontana and C. Baroni). The authors are grateful to all the students, technicians and scientists who contributed to the field activities in the period from 2009 to 2016, the Alpine guides of the Alpinschule of Solda, the helicopter companies Airway, Air Service Center, Star Work Sky and the Hotel Franzenshöhe for logistical support. The authors acknowledge the support of Vinicio Carraro (TeSAF Department of the University of Padova) for the setup of the automatic weather station, and of Umberto Morra di Cella and Paolo Pogliotti (ARPA Val d'Aosta) for the setup of the rock wall temperature dataloggers. The soil surface temperature measured on Mt. Vioz were kindly provided by the Servizio Geologico of the Autonomous province of Trento (Matteo Zumiani).

References

Ballantyne, C. K.: Periglacial geomorphology, John Wiley & Sons Ltd., Hoboken, NJ, USA, 472 pp., ISBN: 978-1-405-10006-9, 2018.

Boeckli, L., Brenning, A., Gruber, S., and Noetzli, J.: Permafrost distribution in the European Alps: Calculation and evaluation of an index map and summary statistics, The Cryosphere, 6, 807–820, https://doi.org/10.5194/tc-6-807-2012, 2012.

Bohleber, P., Wagenbach, D., Schöner, W., and Böhm, R.: To what extent do water isotope records from low accumulation Alpine ice cores reproduce instrumental temperature series?, Tellus B, 65, 1–17, https://doi.org/10.3402/tellusb.v65i0.20148, 2013.

626 Braithwaite, R. J., Zhang, Y., and Raper, S. C. B.: Temperature sensitivity of the mass balance of mountain

627 glaciers and icecaps as a climatological characteristic, Z. Gletsch.kd. Glazialgeol., 38, 35–61 pp., 2002.

628

629 Carturan, L.: Climate change effects on the cryosphere and hydrology of a high-altitude watershed, Ph.D.

630 thesis, TeSAF – University of Padova, 187 pp., 2010.

631

632 Carturan, L., Cazorzi, F., and Dalla Fontana, G.: Distributed mass-balance modelling on two neighbouring

633 glaciers in Ortles-Cevedale Italy, from 2004 to 2009, J. Glaciol., 58, 467–486,

634 https://doi.org/10.3189/2012JoG11J111, 2012a.

635

636 Carturan, L., Dalla Fontana, G., and Borga, M.: Estimation of winter precipitation in a high-altitude catchment

637 of the Eastern Italian Alps: Validation by means of glacier mass balance observations, Geogr. Fis. Din. Quat.,

638 35, 37–48, https://doi.org/10.4461/GFDQ.2012.35.4, 2012b.

639

640 Carturan, L., Filippi, R., Seppi, R., Gabrielli, P., Notarnicola, C., Bertoldi, L., Paul, F., Rastner, P., Cazorzi,

641 F., Dinale, R., and Dalla Fontana, G.: Area and volume loss of the glaciers in the Ortles-Cevedale group

642 (Eastern Italian Alps): controls and imbalance of the remaining glaciers, The Cryosphere, 7, 1339–1359,

643 https://doi.org/10.5194/tc-7-1339-2013, 2013.

644

645 Carturan, L., Cazorzi, F., De Blasi, F., and Dalla Fontana, G.: Air temperature variability over three glaciers

646 in the Ortles–Cevedale (Italian Alps): Effects of glacier fragmentation, comparison of calculation methods,

647 and impacts on mass balance modeling, The Cryosphere, 9(3), 1129– 1146, https://doi.org/10.5194/tc-9-1129-

648 2015, 2015.

649

650 Carturan, L., De Blasi, F., Dinale, R., Dragà, G., Gabrielli, P., Mair, V., Seppi, R., Tonidandel, D., Zanoner,

651 T., Zendrini, T. L., and Dalla Fontana, G.: Data from air, englacial and permafrost temperature measurements

652 on Mt. Ortles (Eastern European Alps) (Version 1.0) [Data set]. Zenodo.

653 https://doi.org/10.5281/zenodo.7879969, 2023.

654

Charbonneau, R., Lardeau, J. P., and Obled, C.: Problems of modelling a high mountainous drainage basin with predominant snow yields, Hydrol. Sci. B., 26, 345–361, https://doi.org/10.1080/02626668109490899, 1981.

Cicoira, A., Beutel, J., Faillettaz, J., Gärtner-Roer, I., and Vieli, A.: Resolving the influence of temperature forcing through heat conduction on rock glacier dynamics: A numerical modelling approach, The Cryosphere, 13, 927–942, https://doi.org/10.5194/tc-13-927-2019, 2019.

Deline, P., Gruber, S., Delaloye, R., Fischer, L., Geertsema, M., Giardino, M., Hasler, A., Kirkbride, M., Krautblatter, M., Magnin, F., McColl, S., Ravanel, L., and Schoeneich, P.: Ice Loss and Slope Stability in High-Mountain Regions, Snow and Ice-Related Hazards, Risks, and Disasters, Academic Press, 521–561, https://doi.org/10.1016/B978-0-12-394849-6.00015-9, 2015.

Gabrielli, P., Carturan, L., Gabrieli, J., Dinale, R., Krainer, K., Hausmann, H., Davis, M., Zagorodnov, V., Seppi, R., Barbante, C., Fontana, G. D., and Thompson, L. G.: Atmospheric warming threatens the untapped glacial archive of Ortles mountain, South Tyrol, J. Glaciol,, 56, 843–853, https://doi.org/10.3189/002214310794457263, 2010.

Gabrielli, P., Barbante, C., Carturan, L., Cozzi, G., Fontana, G. D., Dinale, R., Dragà, G., Gabrieli, J., Kehrwald, N., Mair, V., Thompson, L. G., and Tonidandel, D.: Discovery of cold ice in a new drilling site in the eastern European Alps, Geogr. Fis. Din. Quat., 35, 101–105, https://doi.org/10.4461/GFDQ.2012.35.10, 2012.

Gabrielli, P., Barbante, C., Bertagna, G., Bertó, M., Binder, D., Carton, A., Carturan, L., Cazorzi, F., Cozzi, G., Dalla Fontana, G., Zanoner, T., and Zennaro, P.: Age of the Mt. Ortles ice cores, the Tyrolean Iceman and glaciation of the highest summit of South Tyrol since the Northern Hemisphere Climatic Optimum, The Cryosphere, 10, 2779–2797, https://doi.org/10.5194/tc-10-2779-2016, 2016.

682

683 Guglielmin, M., Aldighieri, B., and Testa, B.: PERMACLIM: A model for the distribution of mountain

684 permafrost, based on climatic observations, Geomorphology, 51, 245–257, https://doi.org/10.1016/S0169-

685 555X(02)00221-0, 2003.

686

687 Harris, C., Arenson, L. U., Christiansen, H. H., Etzelmüller, B., Frauenfelder, R., Gruber, S., Haeberli, W.,

688 Hauck, C., Hölzle, M., Humlum, O., Springman, S. M., and Vonder Mühll, D.: Permafrost and climate in

689 Europe: Monitoring and modelling thermal, geomorphological and geotechnical responses, Earth Sci. Rev.,

690 92, 117–171, https://doi.org/10.1016/j.earscirev.2008.12.002, 2009.

691

692 Huggel, C., Carey, M., Clague, J. J., and Kääb, A.: The high-mountain cryosphere: Environmental changes

693 and human risks, Cambridge University Press, 1–371 pp., https://doi.org/10.1017/CBO9781107588653, 2015.

694

695 Irvine-Fynn, T. and Hubbard, B.: Glacier Hydrology and Runoff, In International Encyclopedia of Geography:

696 People, the Earth, Environment and Technology, Elsevier,

697 https://doi.org/https://doi.org/10.1002/9781118786352.wbieg0709, 2017.

698

699 Kinnard, C., Larouche, O., Demuth, M. N., and Menounos, B.: Modelling glacier mass balance and climate

700 sensitivity in the context of sparse observations: application to Saskatchewan Glacier, western Canada, The

701 Cryosphere, 16, 3071–3099, https://doi.org/10.5194/tc-16-3071-2022, 2022.

702

703 Knight, J. and Harrison, S.: The sensitivity and evolutionary trajectory of the mountain cryosphere:

704 Implications for mountain geomorphic systems and hazards, Land Degrad. Dev.,

705 https://doi.org/10.1002/ldr.4630, 2023.

706

707 Langsdorf, S., Löschke, S., Möller, V., Okem, A., Officer, S., Rama, B., Belling, D., Dieck, W., Götze, S.,

708 Kersher, T., Mangele, P., Maus, B., Mühle, A., Nabiyeva, K., Nicolai, M., Niebuhr, A., Petzold, J., Prentzler,

709 E., Savolainen, J., Scheuffele, H., Weisfeld, S., Weyer, N., Pörtner, H.-O., Roberts, D. C., Tignor, M.,

710 Poloczanska, E. S., Mintenbeck, K., Alegría, A., Craig, M., Langsdorf, S., Löschke, S., Möller, V., Okem, A.,

711 and Rama, B.: IPCC, 2022: Climate Change 2022: Impacts, Adaptation and Vulnerability. Working Group II

712 Contribution to the Sixth Assessment Report of the Intergovernmental Panel on Climate Change, Cambridge

713 University Press, Cambridge, UK and New York, NY, USA, 3056 pp.,

714 https://doi.org/10.1017/9781009325844, 2022.

715

716 Machguth, H., Purves, R. S., Oerlemans, J., Hoelzle, M., and Paul, F.: Exploring uncertainty in glacier mass

717 balance modelling with Monte Carlo simulation, The Cryosphere, 2, 191–204, https://doi.org/10.5194/tc-2-

718 191-2008, 2008.

719

720 Montrasio A, Berra F, Cariboni M, Ceriani M, Deichmann N, Ferliga C, Gregnanin A, Guerra S, Guglielmin

721 M, Jadoul F, Longhin M, Mair V, Mazzoccola D, Sciesa E, and Zappone A: Note illustrative della Carta

722 Geologica d'Italia - Foglio 024 Bormio, ISPRA, Roma, Italy, 16–26 pp., 2012.

723

724 Pepin, N., Bradley, R. S., Diaz, H. F., Baraer, M., Caceres, E. B., Forsythe, N., Fowler, H., Greenwood, G.,

725 Hashmi, M. Z., Liu, X. D., Williamson, S. N., and Yang, D. Q.: Elevation-dependent warming in mountain

726 regions of the world, Nat. Clim. Change, 5, 424–430, https://doi.org/10.1038/nclimate2563, 2015.

727

728 Pepin, N. C., Arnone, E., Gobiet, A., Haslinger, K., Kotlarski, S., Notarnicola, C., Palazzi, E., Seibert, P.,

729 Serafin, S., Schöner, W., Terzago, S., Thornton, J. M., Vuille, M., and Adler, C.: Climate Changes and Their

730 Elevational Patterns in the Mountains of the World, Rev. Geophys., 60,

731 https://doi.org/10.1029/2020RG000730, 2022.

732

733 Shaw, T. E., Buri, P., McCarthy, M., Miles, E. S., Ayala, Á., and Pellicciotti, F.: The Decaying Near-Surface

734 Boundary Layer of a Retreating Alpine Glacier, Geophys. Res. Lett., 50,

735 https://doi.org/10.1029/2023gl103043, 2023.

736

737 Rathore, N., Thakur, D., and Chawla, A.: Seasonal variations coupled with elevation gradient drives significant

738 changes in eco-physiological and biogeochemical traits of a high altitude evergreen broadleaf shrub,

739 Rhododendron anthopogon, Plant Physiol. Bioch., 132, 708–719,

740 https://doi.org/10.1016/J.PLAPHY.2018.08.009, 2018.

741

742 Troxler, P., Ayala, Á., Shaw, T. E., Nolan, M., Brock, B. W., and Pellicciotti, F.: Modelling spatial patterns of

743 near-surface air temperature over a decade of melt seasons on McCall Glacier, Alaska, J. Glaciol., 1–15(257),

744 386– 400, https://doi.org/10.1017/jog.2020.12, 2020.

745

746 World Meteorological Organization: Guide to Instruments and Methods of Observation, Volume I,

747 Measurement of Meteorological Variables (WMO No. 8), Geneva, Switzerland, 2021.

748

749 Zolles, T., Maussion, F., Galos, S. P., Gurgiser, W., and Nicholson, L.: Robust uncertainty assessment of the

750 spatio-temporal transferability of glacier mass and energy balance models, The Cryosphere, 13, 469–489,

751 https://doi.org/10.5194/tc-13-469-2019, 2019.